University of Thessaly
School of Engineering
Department of Mechanical Engineering

Master Thesis

NON-LINEAR HOMOGENIZATION: ELASTOPLASTIC MATERIALS

by

IOANNA PAPADIOTI

Diploma in Civil Engineering, University of Thessaly, 2012

A Thesis
Submitted in Partial Fulfilment of the
Requirements for the Degree of
Master of Science
2013

The approval of the Master Thesis by the Department of Mechanical Engineering, School of Engineering, University of Thessaly does not imply acceptance of the author's views (N. 5343/32 $\alpha\rho$. 202 $\pi\alpha\rho$. 2).

Approved by the Three Members of the Advisory Committee:

First Member *Nikolaos Aravas*
(Supervisor) *Professor of Computational Mechanics,*
Department of Mechanical Engineering, University of Thessaly

Second Member *Gregory Haidemenopoulos*
Professor of Physical Mettalurgy,
Department of Mechanical Engineering, University of Thessaly

Third Member *Alexis Kermanidis*
Assistant Professor of Mechanical Behavior of Metallic Materials,
Department of Mechanical Engineering, University of Thessaly

Acknowledgments

This thesis was carried out at the Laboratory of Mechanics & Strength of Materials under the Master of Science Program of the Department of Mechanical Engineering of University of Thessaly (UTH).

First and foremost I would like to express my deep gratitude to my master thesis advisor, Professor Nikolaos Aravas who was abundantly helpful and offered invaluable assistance, support and guidance. I attribute the level of my Masters degree to his encouragement and effort and without him this dissertation too, would not have been possible. One simply could not wish for a better supervisor.

I would also like to thank the rest of my thesis committee, Professor Gregory Haidemenopoulos and Assistant Professor Alexis Kermanidis for their encouragement and insightful comments.

Last but not least, a thank you to Dr. Kostas Danas, Research Assistant Professor at Laboratoire de Mécanique des Solides (LMS), Ecole Polytechnique, who introduced me to three-dimensional (3-D) finite-element simulations. I am extremely grateful and indebted to him for his expert, sincere and valuable guidance.

Contents

List of Figures

Chapter 1

Introduction

The main objective of homogenization is to predict the macroscopic behaviour of composite materials in terms of the behaviour of their constituents and prescribed statistical information about their microstructure. Homogenization methods are powerful tools for the simulation of the mechanical behavior composites, at a reasonable computational cost. Linking the mechanical response of composites to the underlying microstructure is relevant in a variety of technological applications. One example is the design and the optimization of the forming operations of multiphase metallic alloys.

Historically, emphasis was originally placed on the determination of the elastic constants of a polycrystal from those of a single crystal with first theoretical considerations by Voigt and Reuss. Later, the focus was on the estimation of the effective or overall behavior of linear elastic composite materials. The homogenization methods which were developed include the variational principles of Hashin and Shtrikman (1962), which are particularly well suited to estimate the effective behavior of composites with particulate random microstructures. There is also the self-consistent approximation, developed in several different physical contexts by various authors (e.g., Hershey 1954, Kronër 1958, Willis 1977), which is known to be fairly accurate for polycrystals and other materials with granular microstructures. For nonlinear (e.g., plastic, viscoplastic, etc.) composites, rigorous methods have not been available until fairly recently, even though efforts along these lines have been going on for some time, particularly in the context of ductile polycrystals (e.g., Hill 1965, Hutchinson 1976). Making use of a nonlinear extension of the Hashin-Shtrikman (HS) variational principles, due to Willis (1983), the first bounds of the HS type for nonlinear composites were derived by Talbot and Willis (1985).

Ponte Castañeda (1991) proposed a more general variational approach making use of optimally chosen "linear comparison composites". This approach is not only capable of delivering bounds of the HS type for nonlinear composites, but, in addition, can be used to generate bounds and estimates of other types, such as self-consistent estimates and three-point bounds (Ponte Castañeda 1992). A different, but equivalent method for the special class of power-law materials has been proposed by Suquet (1993). Talbot and Willis (1992) provided a simultaneous generalization of the variational principles of Talbot and Willis (1985) and the linear comparison composite method of Ponte Castañeda (1991), which has the potential to give improved estimates for certain special, non-standard situations.

More recently, Ponte Castañeda (1996, 2002) proposed a second approach that makes use of an "anisotropic composite linear comparison material". While this method does not yield bounds, it appears to give more accurate results.

In the present study we focus on homogenization techniques for non-linear composites that have been developed recently by Ponte Castañeda, Suquet, and co-workers (Ponte-Castañeda 1996, Suquet 1996a, Ponte-Castañeda and Suquet 1998) and their application to two-phase TRIP steels. The implementation of the constitutive model in a general-purpose finite element program and the procedure of solving the problem with finite elements in the context of finite strains are presented. The ABAQUS finite element code provides a general interface so that a particular constitutive model can be introduced via a "user subroutine" named UMAT (User MATerial). The constitutive model developed for the two-phase elastoplastic composite is implemented in ABAQUS through the subroutine UMAT and is used for the analysis of the problem of uniaxial tension.

The Thesis proceeds with Chapter 2, where we develop a methodology for the determination of the plastic part of the deformation rate in elastoplastic materials. We present a description of the homogenization techniques for non-linear materials that has been developed recently by Ponte Castañeda, Suquet, and co-workers. The homogenization techniques are then applied to a two-phase composite.

In Chapter 3, a methodology for the numerical integration of the resulting non-linear constitutive equations for the composite material in the context of the finite element method is presented. The implementation of the constitutive model in a finite element program and the procedure of solving the problem with finite elements in the context of finite strains are presented.

In Chapter 4, the results of the homogenization theory for the two-phase composite are compared to corresponding results of unit cell calculations and finally, in Chapter 5 we compare the above theoretical results of homogenization theory with three-dimensional (3D) calculations of a unit cell with random isotropic distribution of the second phase in the matrix material.

Standard notation is used throughout. Boldface symbols denote tensors the orders of which are indicated by the context. All tensor components are written with respect to a fixed Cartesian coordinate system with base vectors $\mathbf{e}_i$ $(i = 1, 2, 3)$, and the summation convention is used for repeated Latin indices, unless otherwise indicated. The prefice det indicates the determinant, a superscript T the transpose, a superposed dot the material time derivative, and the subscripts s and a the symmetric and anti-symmetric parts of a second order tensor. Let $\mathbf{a}$, $\mathbf{b}$ be vectors, $\mathbf{A}$, $\mathbf{B}$ second-order tensors, and $\mathbf{C}$ a fourth-order tensor; the following products are used in the text $(\mathbf{a}\,\mathbf{b})_{ij} = a_i\,b_j$, $\mathbf{A} : \mathbf{B} = A_{ij}\,B_{ij}$, $(\mathbf{A} \cdot \mathbf{B})_{ij} = A_{ik}\,B_{kj}$, $(\mathbf{A}\,\mathbf{B})_{ijkl} = A_{ij}\,B_{kl}$, $(\mathbf{C} : \mathbf{A})_{ij} = C_{ijkl}\,A_{kl}$, and $(\mathbf{C} : \mathbf{D})_{ijkl} = C_{ijpq}\,D_{pqkl}$. The inverse $\mathbf{C}^{-1}$ of a fourth-order tensor $\mathbf{C}$ that has the "minor" symmetries $C_{ijkl} = C_{jikl} = C_{ijlk}$ is defined so that $\mathbf{C} : \mathbf{C}^{-1} = \mathbf{C}^{-1} : \mathbf{C} = \mathbf{I}$, where $\mathbf{I}$ is the symmetric fourth-order identity tensor with Cartesian components $I_{ijkl} = (\delta_{ik}\,\delta_{jl} + \delta_{il}\,\delta_{jk})/2$, δ_{ij} being the Kronecker delta.

Chapter 2

Theory

2.1 Introduction

The goal of this chapter is to present a methodology for the determination of the plastic behavior of an elastoplastic cpmposite. The total deformation rate $\mathbf{D}$ is written as the sum of an elastic, and a plastic part

$$\mathbf{D} = \mathbf{D}^e + \mathbf{D}^p.$$

The overall plastic behavior of the composite is determined by using a homogenization techniques for non-linear materials that have been developed by Ponte-Castañeda (1996), Suquet (1996a) and Ponte-Castañeda and Suquet (1998).

In this chapter, we present briefly a description of the homogenization technique, which we then apply to a two-phase steel. The homogenization technique is used in order to determine the plastic part of the deformation rate, an equation of the form $\mathbf{D}^p = \mathbf{D}^p(\boldsymbol{\sigma})$. The results of the homogenization for the two-phase composite are compared to those of unit cell calculations in Chapter 4 and to those of 3-D finite-element simulations in Chapter 5.

2.2 Constitutive model of viscoplasticity

Standard isotropic linear hypoelasticity is assumed and the constitutive equation for $\mathbf{D}^e$ is written as

$$\mathbf{D}^e = \boldsymbol{\mathcal{M}}^e : \overset{\triangledown}{\boldsymbol{\sigma}} \qquad \text{or} \qquad \overset{\triangledown}{\boldsymbol{\sigma}} = \boldsymbol{\mathcal{L}}^e : \mathbf{D}^e, \tag{2.1}$$

where $\overset{\triangledown}{\boldsymbol{\sigma}}$ is the Jaumann derivative of the stress tensor $\boldsymbol{\sigma}$, $\boldsymbol{\mathcal{M}}^e$ is the elastic compliance tensor defined as

$$\boldsymbol{\mathcal{M}}^e = \frac{1}{2\,\mu}\,\boldsymbol{\mathcal{K}} + \frac{1}{3\,\kappa}\,\boldsymbol{\mathcal{J}}, \qquad \boldsymbol{\mathcal{L}}^e = \boldsymbol{\mathcal{M}}^{e-1} = 2\,\mu\,\boldsymbol{\mathcal{K}} + 3\,\kappa\,\boldsymbol{\mathcal{J}}, \qquad \boldsymbol{\mathcal{J}} = \frac{1}{3}\,\boldsymbol{\delta}\,\boldsymbol{\delta}, \qquad \boldsymbol{\mathcal{K}} = \boldsymbol{\mathcal{I}} - \boldsymbol{\mathcal{J}}, \tag{2.2}$$

μ and κ denote the elastic shear and bulk moduli, $\boldsymbol{\delta}$ and $\boldsymbol{\mathcal{I}}$ the second- and symmetric fourth-order identity tensors, with Cartesian components δ_{ij} (the Kronecker delta) and $\mathcal{I}_{ijkl} = (\delta_{ik}\,\delta_{jl} + \delta_{il}\,\delta_{jk})/2$.

The rate of the plastic strain using tensor $\mathbf{D}^p$ is given by the form:

$$\mathbf{D}^p = \dot{\bar{\varepsilon}}^p\,\mathbf{N} \qquad \text{with} \qquad \dot{\bar{\varepsilon}}^p = \dot{\varepsilon}_0 \left[\frac{\sigma_{eq}}{\sigma_y\left(\bar{\varepsilon}^p\right)}\right]^m \qquad \text{and} \qquad \mathbf{N} = \frac{3}{2}\frac{\boldsymbol{\sigma}}{\sigma_{eq}}, \qquad (2.3)$$

where $\dot{\varepsilon}_0$ is a reference value for strain rate, m is the strain-rate-sensitivity exponent of the material, $\sigma_{eq} = \sqrt{\frac{3}{2}\mathbf{s}:\mathbf{s}}$ is the von Mises equivalent stress, $\mathbf{s}$ is the deviatoric stress tensor, and $\sigma_y\left(\bar{\varepsilon}^p\right)$ is the yield stress of the material at the reference strain rate $\dot{\varepsilon}_0$. The yield stress of the material exhibits hardening during straining and it is considered as a function of equivalent plastic strain $\bar{\varepsilon}^p$ through:

$$\sigma_y\left(\bar{\varepsilon}^p\right) = \sigma_0 \left(1 + \frac{\bar{\varepsilon}^p}{\varepsilon_0}\right)^{1/n}, \qquad (2.4)$$

where σ_0, ε_0 are reference values for yield stress and strain respectively with $\sigma_0 = E\,\varepsilon_0$ (E is the Young modulus), n is the hardening exponent, and $\bar{\varepsilon}^p = \int_0^t \dot{\bar{\varepsilon}}^p\,dt$ is the equivalent plastic strain. It can be shown easily that the following equations hold

$$\mathbf{N}:\mathbf{N} = \frac{3}{2}, \quad \boldsymbol{\sigma}:\mathbf{N} = \sigma_{eq}, \quad \boldsymbol{\mathcal{L}}^e:\mathbf{N} = \mathbf{N}:\boldsymbol{\mathcal{L}}^e = 2\,G\,\mathbf{N}, \quad \text{and} \quad \sqrt{\frac{2}{3}\mathbf{D}^p:\mathbf{D}^p} = \dot{\bar{\varepsilon}}^p. \quad (2.5)$$

2.3 Homogenization method for non-linear viscous solids

We consider a composite material comprised of N isotropic, viscoplastic and incompressible phases distributed statistically uniformly and isotropically, with dissipation functions of the "power-law" type:

$$U^{(r)}\left(\boldsymbol{\sigma}\right) = \frac{\sigma_0^{(r)}\,\dot{\varepsilon}_0^{(r)}}{n^{(r)}+1}\left(\frac{\sigma_{eq}}{\sigma_0^{(r)}}\right)^{n^{(r)}+1}, \qquad \text{where} \qquad \sigma_{eq} = \sqrt{\frac{3}{2}\,\boldsymbol{\sigma}:\boldsymbol{\sigma}}, \qquad \mathbf{s} = \boldsymbol{\sigma} - \frac{\sigma_{kk}}{3}\boldsymbol{\delta},$$

so that

$$\mathbf{D} = \frac{\partial U^{(r)}}{\partial \boldsymbol{\sigma}} = \dot{\bar{\varepsilon}}^{(r)}\,\mathbf{N} = \frac{\boldsymbol{\sigma}}{2\,\mu^{(r)}\left(\mathbf{s}\right)}, \qquad \dot{\bar{\varepsilon}}^{(r)} = \sqrt{\frac{2}{3}\mathbf{D}:\mathbf{D}} = \dot{\varepsilon}_0^{(r)}\left(\frac{\sigma_{eq}}{\sigma_0^{(r)}}\right)^{n^{(r)}}, \qquad \mathbf{N} = \frac{3}{2\,\sigma_{eq}}\mathbf{s},$$

$$\mu^{(r)}\left(\sigma_{eq}\right) = \frac{1}{3}\frac{\sigma_0^{(r)}}{\dot{\varepsilon}_0^{(r)}}\left(\frac{\sigma_0^{(r)}}{\sigma_{eq}}\right)^{n^{(r)}-1}.$$

There are two interesting limiting cases of the model described above. The first is the linear case, in which $n^{(r)} = 1$:

$$U_L^{(r)} = \frac{\sigma_0^{(r)}\dot{\varepsilon}_0^{(r)}}{2}\left(\frac{\sigma_{eq}}{\sigma_0^{(r)}}\right)^2 = \frac{\sigma_{eq}^2}{6\,\mu^{(r)}}, \qquad \text{where} \qquad \mu^{(r)} = \frac{\sigma_0^{(r)}}{3\,\dot{\varepsilon}_0^{(r)}},$$

and

$$\dot{\bar{\varepsilon}} = \dot{\varepsilon}_0^{(r)}\frac{\sigma_{eq}}{\sigma_0^{(r)}} = \frac{\sigma_{eq}}{3\,\mu^{(r)}}, \qquad \mathbf{D} = \dot{\bar{\varepsilon}}\,\mathbf{N} = \frac{1}{2\,\mu^{(r)}}\mathbf{s}.$$

The second limiting case is perfect plasticity, in which $n^{(r)} \to \infty$. Taking into account that

$$\lim_{n \to \infty} \frac{A^{n+1}}{n+1} = \begin{cases} 0 & \text{when} \quad A \leq 1, \\ \infty & \text{when} \quad A > 1, \end{cases}$$

we conclude that

$$U^{(r)} = \lim_{n \to \infty} \left[\frac{1}{n^{(r)}+1} \sigma_0^{(r)} \dot{\varepsilon}_0^{(r)} \left(\frac{\sigma_{eq}}{\sigma_0^{(r)}} \right)^{n^{(r)}+1} \right] = \begin{cases} 0 & \text{when} \quad \frac{\sigma_{eq}}{\sigma_0^{(r)}} \leq 1, \\ \infty & \text{when} \quad \frac{\sigma_{eq}}{\sigma_0^{(r)}} > 1. \end{cases}$$

In this case $\sigma_0^{(r)}$ is the classical yield stress of the perfectly plastic material.
Our goal is to draw an expression for the dissipation function in order to be able to derive the equivalent plastic strain for the composite material.
The dissipation function of the composite is defined by (Ponte: i) JMPS 1991, eqns (3.6) & (3.2), ii) Advances 1998, eq (4.52), iii) Udine 1997, eqns (5.18) & (5.19))

$$\tilde{U}(\bar{\boldsymbol{\sigma}}) = \sup_{\mu^{(r)} \geq 0} \left\{ \tilde{U}_L\left(\bar{\sigma}_{eq}, \tilde{\mu}\left(\mu^{(r)} \right) \right) - \sup_{\sigma_{eq}^{(r)} \geq 0} \sum_{r=1}^{N} c^{(r)} \left[U_L^{(r)}\left(\sigma_{eq}^{(r)}, \mu^{(r)} \right) - U^{(r)}\left(\sigma_{eq}^{(r)} \right) \right] \right\}, \quad (2.6)$$

where

$$\tilde{U}_L = \frac{\bar{\sigma}_{eq}^2}{6\,\tilde{\mu}\left(\mu^{(r)} \right)}, \qquad U_L^{(r)} = \frac{\sigma_{eq}^{(r)2}}{6\,\mu^{(r)}}. \tag{2.7}$$

In the above expressions U_L is the dissipation function of a "linear comparison" material with effective modulus $\tilde{\mu}$.
The corresponding constitutive equation for the composite is

$$\bar{\mathbf{D}} = \frac{\partial \tilde{U}}{\partial \bar{\boldsymbol{\sigma}}}.$$

Optimization of (2.6) with respect to $\sigma_{eq}^{(r)}$:

$$\frac{\partial \tilde{U}}{\partial \sigma_{eq}^{(r)}} = \frac{\partial}{\partial \sigma_{eq}^{(r)}} \left\{ \sum_{s=1}^{N} c^{(s)} \left[U_L^{(s)}\left(\sigma_{eq}^{(s)}, \mu^{(s)} \right) - U^{(s)}\left(\sigma_{eq}^{(s)} \right) \right] \right\} = c^{(r)} \left(\frac{\sigma_{eq}^{(r)}}{3\,\mu^{(r)}} - \frac{\partial U^{(r)}}{\partial \sigma_{eq}^{(r)}} \right) =$$

$$= c^{(r)} \left[\frac{\sigma_{eq}^{(r)}}{3\,\mu^{(r)}} - \dot{\varepsilon}_0^{(r)} \left(\frac{\sigma_{eq}^{(r)}}{\sigma_0^{(r)}} \right)^{n^{(r)}} \right] = 0 \quad \Rightarrow \quad \sigma_{eq}^{(r)} = \left[\frac{\sigma_0^{(r)n^{(r)}}}{3\,\mu^{(r)}\,\dot{\varepsilon}_0^{(r)}} \right]^{\frac{1}{n^{(r)}-1}} \equiv \hat{\sigma}_{eq}^{(r)}. \tag{2.8}$$

Substituting $\sigma_{eq}^{(r)} = \hat{\sigma}_{eq}^{(r)}$ in (2.6), we find

$$\tilde{U}(\bar{\boldsymbol{\sigma}}) = \sup_{\mu^{(r)} \geq 0} \left[\frac{\bar{\sigma}_{eq}^2}{6\,\tilde{\mu}\left(\mu^{(r)} \right)} - \frac{1}{2} \sum_{r=1}^{N} \frac{n^{(r)}-1}{n^{(r)}+1} \left(\frac{\sigma_0^{(r)n^{(r)}}}{\dot{\varepsilon}_0^{(r)}} \right)^{\frac{2}{n^{(r)}-1}} \frac{c^{(r)}}{\left(3\,\mu^{(r)} \right)^{\frac{n^{(r)}+1}{n^{(r)}-1}}} \right]. \tag{2.9}$$

The effective modulus $\tilde{\mu}$ for particulate composites is estimated in terms of a reference modulus μ_0 as

$$\tilde{\mu}\left(\mu^{(r)}\right) = \frac{\sum\limits_{s=1}^{N} \frac{c^{(s)}\mu^{(s)}}{3\mu_0+2\mu^{(s)}}}{\sum\limits_{r=1}^{N} \frac{c^{(r)}}{3\mu_0+2\mu^{(r)}}}$$

or

$$\frac{\mu^{(1)}}{\tilde{\mu}} = \frac{\sum\limits_{r=1}^{N} \frac{c^{(r)}y^{(r)}}{3\frac{y^{(r)}}{y_0+2}}}{\sum\limits_{s=1}^{N} \frac{c^{(s)}}{3\frac{y^{(s)}}{y_0}+2}} \equiv \frac{T_1\left(y^{(i)}\right)}{T_2\left(y^{(i)}\right)} \equiv F\left(y^{(i)}\right), \tag{2.10}$$

where $\qquad y^{(r)} = \frac{\mu^{(1)}}{\mu^{(r)}} \quad \left(y^{(1)} = 1\right) \qquad$ and $\qquad y_0 = \frac{\mu^{(1)}}{\mu_0} = y_0\left(y^{(r)}\right).$

Note that

$$\frac{3}{y_0}T_1 + 2T_2 = \sum_{r=1}^{N} \frac{3\frac{y^{(r)}}{y_0}c^{(r)}}{3\frac{y^{(r)}}{y_0}+2} + \sum_{r=1}^{N} \frac{2c^{(r)}}{3\frac{y^{(r)}}{y_0}+2} = \sum_{r=1}^{N} \frac{3\frac{y^{(r)}}{y_0}c^{(r)}+2c^{(r)}}{3\frac{y^{(r)}}{y_0}+2} =$$

$$= \sum_{r=1}^{N} \frac{\left(3\frac{y^{(r)}}{y_0}+2\right)c^{(r)}}{3\frac{y^{(r)}}{y_0}+2} \quad \Rightarrow$$

$$3\frac{T_1}{y_0} + 2T_2 = \sum_{r=1}^{N} c^{(r)}, \quad T_1 = \frac{y_0}{3}\left(\sum_{r=1}^{N} c^{(r)} - 2T_2\right), \quad T_2 = \frac{1}{2}\left(\sum_{r=1}^{N} c^{(r)} - \frac{3}{y_0}T_1\right). \tag{2.11}$$

At this point we treat the $c^{(r)}$'s as independent variables, so that

$$\frac{\partial T_1}{\partial c^{(i)}} = \frac{\partial y_0}{\partial c^{(i)}}\underbrace{\frac{1}{3}\left(\sum_{r=1}^{N} c^{(r)} - 2T_2\right)}_{T_1/3} + \frac{y_0}{3}\left(1 - 2\frac{\partial T_2}{\partial c^{(i)}}\right) \Rightarrow \frac{\partial T_1}{\partial c^{(i)}} = \frac{T_1}{y_0}\frac{\partial y_0}{\partial c^{(i)}} + \frac{y_0}{3}\left(1 - 2\frac{\partial T_2}{\partial c^{(i)}}\right).$$

The constraint $\sum\limits_{r=1}^{N} c^{(r)} = 1$ is taken care of by the constitutive equations.

The reference modulus can be chosen in various ways as follows:

i) $\mu_0 = \mu^{(1)}$ (Hashin-Shtrikman)

$$y_0 = 1 \quad \Rightarrow \quad \frac{\partial y_0}{\partial y^{(r)}} = 0, \tag{2.12}$$

ii) $\mu_0 = \sum\limits_{r=1}^{N} c^{(r)}\mu^{(r)}$ (Voigt model)

$$\frac{1}{y_0} = \frac{\mu_0}{\mu^{(1)}} = \sum_{r=1}^{N} c^{(r)}\frac{\mu^{(r)}}{\mu^{(1)}} = \sum_{r=1}^{N} \frac{c^{(r)}}{y^{(r)}} \Rightarrow -\frac{1}{y_0^2}\frac{\partial y_0}{\partial y^{(i)}} = -\frac{c^{(i)}}{y^{(i)2}} \Rightarrow \frac{\partial y_0}{\partial y^{(i)}} = c^{(i)}\left(\frac{y_0}{y^{(i)}}\right)^2, \tag{2.13}$$

iii) $\frac{1}{\mu_0} = \sum\limits_{r=1}^{N} \frac{c^{(r)}}{\mu^{(r)}}$ (Reuss model)

$$y_0 = \frac{\mu^{(1)}}{\mu_0} = \sum_{r=1}^{N} c^{(r)} \frac{\mu^{(1)}}{\mu^{(r)}} = \sum_{r=1}^{N} c^{(r)} y^{(r)} \quad \Rightarrow \quad \frac{\partial y_0}{\partial y^{(i)}} = y^{(i)}, \qquad (2.14)$$

iv) Self-consistent scheme

$$\mu_0 = \frac{\sum\limits_{s=1}^{N} \frac{c^{(s)} \mu^{(s)}}{3\mu_0 + 2\mu^{(s)}}}{\sum\limits_{r=1}^{N} \frac{c^{(r)}}{3\mu_0 + 2\mu^{(r)}}} \quad \Rightarrow \quad \frac{1}{\mu_0} = \frac{\sum\limits_{r=1}^{N} \frac{c^{(r)}}{3\mu_0 + 2\mu^{(r)}}}{\sum\limits_{s=1}^{N} \frac{c^{(s)} \mu^{(s)}}{3\mu_0 + 2\mu^{(s)}}} \quad \Rightarrow$$

$$\frac{\mu^{(1)}}{\mu_0} = \frac{\sum\limits_{r=1}^{N} \frac{c^{(r)}}{3\frac{\mu_0}{\mu^{(1)}} + 2\frac{\mu^{(r)}}{\mu^{(1)}}}}{\sum\limits_{s=1}^{N} \frac{c^{(s)}\frac{\mu^{(s)}}{\mu^{(1)}}}{3}\frac{\mu_0}{\mu^{(1)}} + 2\frac{\mu^{(s)}}{\mu^{(1)}}} \quad \Rightarrow \quad y_0 = \frac{\sum\limits_{r=1}^{N} \frac{c^{(r)}}{\frac{3}{y_0} + \frac{2}{y^{(r)}}}}{\sum\limits_{s=1}^{N} \frac{\frac{c^{(s)}}{y^{(s)}}}{\frac{3}{y_0} + \frac{2}{y^{(s)}}}}. \qquad (2.15)$$

The last equation is solve numerically for y_0.

In this thesis for the calculations we use Reuss model, and we compare the results with the ones for $\mu_0 = \mu^{(1)}$ (Hashin-Shtrikman), the unit cell calculations and the 3-D finite-element simulations.

Continuing with the calculations, we substitute from (2.10) into (2.9) and we find

$$\tilde{U} = \sup_{\substack{y^{(r)} \geq 0 \\ y^{(1)} = 1}} \sup_{\mu^{(1)} > 0} \left[\frac{\bar{\sigma}_{eq}^2}{6\,\mu^{(1)}} F\left(y^{(r)}\right) - I\left(\mu^{(1)}, y^{(r)}\right) \right], \qquad (2.16)$$

where

$$I\left(\mu^{(1)}, y^{(r)}\right) = \frac{1}{2} \sum_{r=1}^{N} c^{(r)} \frac{n^{(r)} - 1}{n^{(r)} + 1} \left(\frac{\sigma_0^{(r)^{n^{(r)}}}}{\dot{\varepsilon}_0^{(r)}} \right)^{\frac{2}{n^{(r)} - 1}} \left(\frac{y^{(r)}}{3\,\mu^{(1)}} \right)^{\frac{n^{(r)} + 1}{n^{(r)} - 1}}. \qquad (2.17)$$

Optimization of (2.16) with respect to $\mu^{(1)}$:

$$\frac{\partial \tilde{U}}{\partial \mu^{(1)}} = -\frac{1}{6} \left[F \left(\frac{\bar{\sigma}_{eq}}{\mu^{(1)}} \right)^2 + 6\frac{\partial I}{\partial \mu^{(1)}} \right] = 0, \qquad (2.18)$$

where

$$\frac{\partial I}{\partial \mu^{(1)}} = -\frac{3}{2} \sum_{r=1}^{N} c^{(r)} \left(\frac{\sigma_0^{(r)^{n^{(r)}}}}{\dot{\varepsilon}_0^{(r)}} \right)^{\frac{2}{n^{(r)} - 1}} \frac{y^{(r)^{\frac{n^{(r)} + 1}{n^{(r)} - 1}}}}{\left(3\,\mu^{(1)} \right)^{\frac{2\,n^{(r)}}{n^{(r)} - 1}}},$$

so that (2.18) becomes

$$F\left(y^{(r)}\right)\left(\frac{\bar{\sigma}_{eq}}{\mu^{(1)}}\right)^2 - 9\sum_{r=1}^{N} c^{(r)} \left(\frac{\sigma_0^{(r)^{n(r)}}}{\dot{\varepsilon}_0^{(r)}}\right)^{\frac{2}{n^{(r)}-1}} \frac{y^{(r)^{\frac{n^{(r)}+1}{n^{(r)}-1}}}}{\left(3\,\mu^{(1)}\right)^{\frac{2\,n^{(r)}}{n^{(r)}-1}}} = 0$$

or

$$F\left(y^{(r)}\right)\bar{\sigma}_{eq}^2 - \sum_{r=1}^{N} c^{(r)} \left(\frac{\sigma_0^{(r)^{n(r)}}}{3\,\mu^{(1)}\,\dot{\varepsilon}_0^{(r)}}\right)^{\frac{2}{n^{(r)}-1}} y^{(r)^{\frac{n^{(r)}+1}{n^{(r)}-1}}} = 0,$$

which yields

$$\mu^{(1)} = \frac{1}{3}\left[\frac{1}{F\left(y^{(r)}\right)\bar{\sigma}_{eq}^2}\sum_{r=1}^{N} c^{(r)} \left(\frac{\sigma_0^{(r)^{n(r)}}}{\dot{\varepsilon}_0^{(r)}}\right)^{\frac{2}{n^{(r)}-1}} y^{(r)^{\frac{n^{(r)}+1}{n^{(r)}-1}}}\right]^{\frac{n^{(r)}-1}{2}} > 0. \qquad (2.19)$$

The last equation defines $\mu^{(1)}$ in terms of $\bar{\sigma}_{eq}$ and the $y^{(r)}$. Note that the definition of $\mu^{(1)}$ is consistent with the constraint $\mu^{(1)} > 0$.

For those $y^{(r)} > 0$, i.e., $y^{(r)} \neq 0$, optimization of (2.16) with respect to $y^{(r)}$ yields:

$$\frac{\partial \tilde{U}}{\partial y^{(r)}} = \frac{\partial F}{\partial y^{(r)}} \frac{\bar{\sigma}_{eq}^2}{6\,\mu^{(1)}} - \frac{\partial I}{\partial y^{(r)}} = 0, \qquad r = 2, 3, \cdots, N. \qquad (2.20)$$

Since

$$\frac{\partial I}{\partial y^{(i)}} = \frac{1}{2}\frac{c^{(i)}}{\left(3\,\mu^{(1)}\right)^{\frac{n^{(i)}+1}{n^{(i)}-1}}} \left(\frac{y^{(i)}\,\sigma_0^{(i)^{n(i)}}}{\dot{\varepsilon}_0^{(i)}}\right)^{\frac{2}{n^{(i)}-1}},$$

the optimality condition (2.20) becomes

$$\frac{\partial F}{\partial y^{(i)}} \bar{\sigma}_{eq}^2 \left(3\,\mu^{(1)}\right)^{\frac{2}{n^{(i)}-1}} - c^{(i)} \left(\frac{y^{(i)}\,\sigma_0^{(i)^{n(i)}}}{\dot{\varepsilon}_0^{(i)}}\right)^{\frac{2}{n^{(i)}-1}} = 0, \qquad i = 2, 3, \cdots, N. \qquad (2.21)$$

Equations (2.19) and (2.21) define the optimal values $\mu^{(1)} = \hat{\mu}^{(1)}\left(\bar{\sigma}_{eq}, c^{(s)}, \sigma_0^{(s)}\right)$ and $y^{(r)} = \hat{y}^{(r)}\left(\bar{\sigma}_{eq}, c^{(s)}, \sigma_0^{(s)}\right)$.

The composite dissipation function is defined from (2.16):

$$\tilde{U}\left(\bar{\sigma}_{eq}\right) = \frac{1}{6}\frac{F\left(\hat{y}^{(r)}\left(\bar{\sigma}_{eq}\right)\right)}{\hat{\mu}^{(1)}\left(\bar{\sigma}_{eq}\right)} \bar{\sigma}_{eq}^2 - I\left(\hat{\mu}^{(1)}\left(\bar{\sigma}_{eq}\right), \hat{y}^{(r)}\left(\bar{\sigma}_{eq}\right)\right), \qquad (2.22)$$

and the flow rule is

$$\bar{\mathbf{D}} = \frac{\partial \tilde{U}}{\partial \bar{\boldsymbol{\sigma}}} = \frac{\partial \tilde{U}}{\partial \bar{\sigma}_{eq}}\frac{\partial \bar{\sigma}_{eq}}{\partial \bar{\mathbf{s}}} \equiv \dot{\bar{\varepsilon}}\,\mathbf{N}, \qquad \dot{\bar{\varepsilon}} = \frac{\partial \tilde{U}}{\partial \bar{\sigma}_{eq}}, \qquad \mathbf{N} = \frac{\partial \bar{\sigma}_{eq}}{\partial \bar{\boldsymbol{\sigma}}} = \frac{3}{2\,\bar{\sigma}_{eq}}\bar{\mathbf{s}}.$$

Using (2.22), we find that

$$\dot{\bar{\varepsilon}} = \frac{\partial \tilde{U}}{\partial \bar{\sigma}_{eq}} = \underbrace{F}_{\frac{\hat{\mu}^{(1)}}{\tilde{\mu}}} \frac{\bar{\sigma}_{eq}}{3\,\hat{\mu}^{(1)}} + \underbrace{\frac{\partial \tilde{U}}{\partial \hat{\mu}^{(1)}}}_{0} \frac{\partial \hat{\mu}^{(1)}}{\partial \bar{\sigma}_{eq}} + \sum_{i=1}^{N} \underbrace{\frac{\partial \tilde{U}}{\partial \hat{y}^{(i)}}}_{0} \frac{\partial \hat{y}^{(i)}}{\partial \bar{\sigma}_{eq}} = \frac{\bar{\sigma}_{eq}}{3\,\tilde{\mu}},$$

where the partial derivatives $\frac{\partial \tilde{U}}{\partial \hat{\mu}^{(1)}}$ and $\frac{\partial \tilde{U}}{\partial \hat{y}^{(i)}}$ vanish due to the optimization conditions (2.18) and (2.20).

The flow rule now takes the form

$$\bar{\mathbf{D}} = \dot{\bar{\varepsilon}}\,\mathbf{N} = \frac{\bar{\sigma}_{eq}}{3\,\tilde{\mu}}\,\mathbf{N} = \frac{\bar{\boldsymbol{\sigma}}}{2\,\tilde{\mu}}, \qquad \tilde{\mu} = \tilde{\mu}\left(\hat{\mu}^{(r)}\right), \quad \text{and} \quad \hat{\mu}^{(r)} = \frac{\hat{\mu}^{(1)}\left(\bar{\sigma}_{eq}, c^{(s)}, \sigma_0^{(s)}\right)}{\hat{y}^{(r)}\left(\bar{\sigma}_{eq}, c^{(s)}, \sigma_0^{(s)}\right)}. \qquad (2.23)$$

In the following we examine first the form of the dissipation function and the flow rule when all creep exponents are equal to n, and then consider the limit of perfect plasticity $n \to \infty$.

2.4   The case where all creep exponents are equal

We consider the special case where all creep exponents are equal $\left(n^{(1)} = n^{(2)} = \cdots = n^{(N)} = n\right)$. The dissipation function of the composite given by equation (2.9) of the previous section takes the form

$$\tilde{U} = \sup_{\mu^{(r)} \geq 0} \left[\frac{\bar{\sigma}_{eq}^2}{6\,\tilde{\mu}\left(\mu^{(r)}\right)} - \frac{n-1}{2\,(n+1)} \sum_{r=1}^{N} \frac{c^{(r)}}{\left(3\,\mu^{(r)}\right)^{\frac{n+1}{n-1}}} \left(\frac{\sigma_0^{(r)n}}{\dot{\varepsilon}_0^{(r)}}\right)^{\frac{2}{n-1}} \right],$$

which can be written also as

$$\tilde{U} = \sup_{\substack{y^{(r)} \geq 0 \\ y^{(1)} = 1}} \sup_{\mu^{(1)} > 0} \left[\frac{\bar{\sigma}_{eq}^2}{6\,\mu^{(1)}} F\left(y^{(r)}\right) - \frac{n-1}{2(n+1)} \frac{H\left(y^{(r)}\right)}{\left(3\,\mu^{(1)}\right)^{\frac{n+1}{n-1}}} \right], \qquad (2.24)$$

where now

$$F\left(y^{(r)}\right) = \frac{\mu^{(1)}}{\tilde{\mu}} = \frac{\displaystyle\sum_{r=1}^{N} \frac{c^{(r)}\,y^{(r)}}{3^{\frac{y^{(r)}}{y_0}+2}}}{\displaystyle\sum_{s=1}^{N} \frac{c^{(s)}}{3^{\frac{y^{(s)}}{y_0}+2}}} \equiv \frac{T_1}{T_2} \quad \text{and} \quad H\left(y^{(r)}\right) = \sum_{r=1}^{N} c^{(r)} \left(\frac{\sigma_0^{(r)n}}{\dot{\varepsilon}_0^{(r)}}\right)^{\frac{2}{n-1}} \left(y^{(r)}\right)^{\frac{n+1}{n-1}}.$$

The optimality conditions (2.19) and (2.21) of the previous section take now the form

$$\mu^{(1)} = \frac{1}{3} \left[\frac{H\left(y^{(r)}\right)}{F\left(y^{(r)}\right)} \frac{1}{\bar{\sigma}_{eq}^2} \right]^{\frac{n-1}{2}} \equiv \hat{\mu}^{(1)}\left(y^{(r)}\right),$$

$$\frac{\partial F}{\partial y^{(i)}}\,\bar{\sigma}_{eq}^2\,\left(3\,\mu^{(1)}\right)^{\frac{2}{n^{(i)}-1}} - c^{(i)} \left(\frac{y^{(i)}\sigma_0^{(i)n^{(i)}}}{\dot{\varepsilon}_0^{(i)}}\right)^{\frac{2}{n^{(i)}-1}} = 0, \qquad i = 2, 3, \cdots, N. \quad (2.25)$$

Substituting the optimal value of from (2.25) in (2.25) we get

$$\frac{\partial F}{\partial y^{(i)}}\frac{H}{F} - c^{(i)}\left(\frac{y^{(i)}\sigma_0^{(i)^n}}{\dot{\varepsilon}_0^{(i)}}\right)^{\frac{2}{n-1}} = 0, \qquad i = 2, 3, \cdots, N. \tag{2.26}$$

Equations (2.26) that define the optimal values of $\hat{y}^{(i)} = \hat{y}^{(i)}\left(c^{(r)}, \sigma_0^{(r)}\right)$ are independent of $\bar{\sigma}_{eq}$. This means that the optimal values $\hat{y}^{(i)} = \hat{y}^{(i)}\left(c^{(r)}, \sigma_0^{(r)}\right)$ are also independent of $\bar{\sigma}_{eq}$.

Substituting the optimal value of $\mu^{(1)} = \hat{\mu}^{(1)}\left(y^{(r)}\right)$ from (2.24) in (2.21), we find that

$$\tilde{U} = \frac{\bar{\sigma}_{eq}^{n+1}}{n+1}\sqrt{\sup_{y^{(r)}\geq 0}\left\{\frac{\left[F\left(y^{(r)}\right)\right]^{n+1}}{\left[H\left(y^{(r)}\right)\right]^{n-1}}\right\}} = \frac{1}{n+1}\underbrace{\sqrt{\frac{F\left(\hat{y}^{(r)}\right)^{n+1}}{H\left(\hat{y}^{(r)}\right)^{n-1}}}}_{\dot{\bar{\varepsilon}}_0/\bar{\sigma}_0^n}\;\bar{\sigma}_{eq}^{n+1}. \tag{2.27}$$

2.5 Perfect plasticity

Next, we consider the case of perfect plasticity, i.e., we take the limit $n \to \infty$. We write the dissipation function (2.27) in the form

$$\tilde{U} = \frac{1}{n+1}\left\{\bar{\sigma}_{eq}^2 \sup_{\substack{y^{(r)}\geq 0\\ y^{(1)}=1}}\left[\frac{F\left(y^{(r)}\right)^{\frac{n-1}{n+1}}}{H\left(y^{(r)}\right)}\right]\right\}^{\frac{n+1}{2}}$$

and taking into account that

$$\lim_{x\to\infty}\left\{\left[\frac{a\left(x\right)}{x}\right]^{x/2}\right\} = \begin{cases} 0 & \text{when} \quad a\left(\infty\right) \leq 1, \\ \infty & \text{when} \quad a\left(\infty\right) > 1. \end{cases}$$

Then, we conclude that

$$\lim_{n\to\infty}\tilde{U} = \begin{cases} 0 & \text{when} \quad \bar{\sigma}_{eq}^2 \sup_{\substack{y^{(r)}\geq 0\\ y^{(1)}=1}}\left[\frac{F\left(y^{(r)}\right)}{H^\infty\left(y^{(r)}\right)}\right] \leq 1, \\ \infty & \text{when} \quad \bar{\sigma}_{eq}^2 \sup_{\substack{y^{(r)}\geq 0\\ y^{(1)}=1}}\left[\frac{F\left(y^{(r)}\right)}{H^\infty\left(y^{(r)}\right)}\right] > 1, \end{cases} \tag{2.28}$$

where

$$F\left(y^{(r)}\right) = \frac{\mu^{(1)}}{\tilde{\mu}} = \frac{\displaystyle\sum_{r=1}^{N}\frac{c^{(r)}y^{(r)}}{3^{\frac{y^{(r)}}{y_0}+2}}}{\displaystyle\sum_{s=1}^{N}\frac{c^{(s)}}{3^{\frac{y^{(s)}}{y_0}+2}}} \equiv \frac{T_1}{T_2}, \qquad H_\infty\left(y^{(r)}\right) \equiv \lim_{n\to\infty}H\left(y^{(r)}\right) = \sum_{r=1}^{N}c^{(r)}\left(\sigma_0^{(r)}\right)^2 y^{(r)}. \tag{2.29}$$

The threshold of the function in (2.28) corresponds to the definition of the effective yield function, i.e.,

$$\bar{\sigma}_{eq}^2 \sup_{\substack{y^{(r)}\geq 0 \\ y^{(1)}=1}} \left[\frac{F\left(y^{(r)}\right)}{H_\infty\left(y^{(r)}\right)} \right] = 1 \qquad \Rightarrow$$

$$\bar{\sigma}_{eq}^2 = \frac{1}{\sup\limits_{\substack{y^{(r)}\geq 0 \\ y^{(1)}=1}} \left[\frac{F\left(y^{(r)}\right)}{H_\infty\left(y^{(r)}\right)} \right]} = \inf_{\substack{y^{(r)}\geq 0 \\ y^{(1)}=1}} \left[\frac{H_\infty\left(y^{(r)}\right)}{F\left(y^{(r)}\right)} \right] = -\sup_{\substack{y^{(r)}\geq 0 \\ y^{(1)}=1}} \left[-\frac{H_\infty\left(y^{(r)}\right)}{F\left(y^{(r)}\right)} \right] \equiv \bar{\sigma}_0^2.$$

This leads to the conclusion that the yield function can be written in the form

$$\tilde{\Phi}\left(\bar{\sigma}_{eq}\right) = \bar{\sigma}_{eq} - \bar{\sigma}_0 = 0, \qquad \bar{\sigma}_0 = \sqrt{\inf_{\substack{y^{(r)}\geq 0 \\ y^{(1)}=1}} \left[\frac{H_\infty\left(y^{(r)}\right)}{F\left(y^{(r)}\right)} \right]}. \tag{2.30}$$

The flow stress $\bar{\sigma}_0$ is written in the form

$$\bar{\sigma}_0 = \sqrt{\inf_{\substack{y^{(r)}\geq 0 \\ y^{(1)}=1}} \left[\frac{\sum\limits_{t=1}^{N} c^{(t)} \sigma_0^{(t)^2} y^{(t)}}{\left(\sum\limits_{r=1}^{N} \frac{c^{(r)} y^{(r)}}{3\frac{y^{(r)}}{y_0}+2} \right) \left(\sum\limits_{s=1}^{N} \frac{c^{(s)}}{3\frac{y^{(s)}}{y_0}+2} \right)^{-1}} \right]} \equiv \sqrt{\frac{H_\infty\left(\hat{y}^{(r)}\right)}{F\left(\hat{y}^{(r)}\right)}}, \tag{2.31}$$

where $H_\infty\left(y^{(r)}\right)$ and $F\left(y^{(r)}\right)$ are defined in (2.29) and $\hat{y}^{(r)} = \hat{y}^{(r)}\left(c^{(s)}, \sigma_0^{(s)}\right)$ are the optimal values.

Essentially we are dealing with a von-Mises-type of yield function (2.30) with an effective flow stress $\bar{\sigma}_0$ defined by (2.31).

Depending on the parameters of the problem, the optimal values $\hat{y}^{(r)} = \frac{\hat{\mu}^{(1)}}{\hat{\mu}^{(r)}}$ may take one of the extreme values 0 or ∞ (rigid or incompressible-void comparison material). In the limit of $\sigma_0^{(r)} \to 0$ (incompressible-void phase), the optimal value $\hat{y}^{(r)} = \frac{\hat{\mu}^{(1)}}{\hat{\mu}^{(r)}} \to \infty$ (incompressible-void comparison material), in such a way that $\sigma_0^{(r)^2} y^{(r)} \to 0$; i.e., an incompressible void phase requires an incompressible void comparison material. On the other hand, it is possible to have $\hat{y}^{(r)} = \frac{\hat{\mu}^{(1)}}{\hat{\mu}^{(r)}} = 0$ (rigid comparison material) even for finite $\sigma_0^{(r)}$ (Ponte Castañeda and de Botton, 1992); in this case obviously $\sigma_0^{(r)^2} y^{(r)} = 0$ again.

The stationarity conditions in (2.31) and the variation of $\bar{\sigma}_0$ with respect to $c^{(i)}$ and $\sigma_0^{(i)}$ are discussed in Appendix A.

2.6 Strain-concentration tensors $\mathbf{A}^{(r)}$

Let the reference matrix material be denoted by phase 0, whereas the inclusion phases are labeled as phases $1, 2, ..., N$. Each phase r is described by an isotropic elastic modulus

$$\boldsymbol{\mathcal{L}}^{(r)} = 3\,\kappa^{(r)}\,\boldsymbol{\mathcal{J}} + 2\,\mu^{(r)}\,\boldsymbol{\mathcal{K}}, \tag{2.32}$$

such that

$$\boldsymbol{\mathcal{L}}^{(r)} - \boldsymbol{\mathcal{L}}^{(0)} = 2\left(\mu^{(r)} - \mu_0\right)\boldsymbol{\mathcal{K}} + 3\left(\kappa^{(r)} - \kappa_0\right)\boldsymbol{\mathcal{J}},$$

where $\mu^{(r)}$ and $\kappa^{(r)}$ correspond to the shear and bulk modulus of the phase r. Making use of the orthogonality of the fourth order tensors $\boldsymbol{\mathcal{K}}$ and $\boldsymbol{\mathcal{J}}$, we conclude that

$$\boldsymbol{\mathcal{M}}^{(r)} = \boldsymbol{\mathcal{L}}^{(r)^{-1}} = \frac{1}{2\,\mu^{(r)}}\boldsymbol{\mathcal{K}} + \frac{1}{3\,\kappa^{(r)}}\boldsymbol{\mathcal{J}}. \tag{2.33}$$

For an isotropic and uniform distribution of spherical inclusion phases, we have that the deformation rate $\mathbf{D}^{(r)}$ in each inclusion is related to the macroscopic deformation rate $\mathbf{D}$ by an equation of the form (Willis, 1977, 1998)

$$\mathbf{D}^{(r)} = \mathbf{E}^{(r)} : \mathbf{D} \qquad \text{with} \qquad \mathbf{E}^{(r)} = \left[\boldsymbol{\mathcal{I}} + \mathbf{P}^{(r)} : \left(\boldsymbol{\mathcal{L}}^{(r)} - \boldsymbol{\mathcal{L}}^{(0)}\right)\right]^{-1}, \tag{2.34}$$

where

$$\mathbf{P}^{(r)} = \mathbf{S}^{(r)} : \boldsymbol{\mathcal{M}}^{(0)}, \qquad \mathbf{S}^{(r)} = \frac{6\left(\kappa_0 + 2\,\mu_0\right)}{5\left(3\,\kappa_0 + 4\,\mu_0\right)}\boldsymbol{\mathcal{K}} + \frac{3\,\kappa_0}{3\,\kappa_0 + 4\,\mu_0}\boldsymbol{\mathcal{J}}. \tag{2.35}$$

Then

$$\mathbf{P}^{(r)} = \frac{3\left(\kappa_0 + 2\,\mu_0\right)}{5\,\mu_0\left(3\,\kappa_0 + 4\,\mu_0\right)}\boldsymbol{\mathcal{K}} + \frac{1}{3\,\kappa_0 + 4\,\mu_0}\boldsymbol{\mathcal{J}} \qquad r = 2, ..., N. \tag{2.36}$$

The Eshelby solution of the inclusion problem gives

$$\mathbf{D}^{(r)} = \mathbf{E}^{(r)} : \mathbf{D} \qquad \text{with} \qquad \mathbf{E}^{(r)} = \left[\boldsymbol{\mathcal{I}} + \mathbf{P}^{(r)} : \left(\boldsymbol{\mathcal{L}}^{(r)} - \boldsymbol{\mathcal{L}}^{(0)}\right)\right]^{-1}.$$

We also compute the following for phase r :

$$\boldsymbol{\mathcal{I}} + \mathbf{P}^{(r)} : \left(\boldsymbol{\mathcal{L}}^{(r)} - \boldsymbol{\mathcal{L}}^{(0)}\right) =$$

$$= \left[1 + \left(\mu^{(r)} - \mu_0\right)\frac{6\left(\kappa_0 + 2\,\mu_0\right)}{5\,\mu^{(1)}\left(3\,\kappa_0 + 4\,\mu_0\right)}\right]\boldsymbol{\mathcal{K}} + \left[1 + \frac{3\left(\kappa^{(r)} - \kappa_0\right)}{3\,\kappa_0 + 4\,\mu_0}\right]\boldsymbol{\mathcal{J}} =$$

$$= \frac{\mu_0\left(9\,\kappa_0 + 8\,\mu_0\right) + 6\left(\kappa_0 + 2\,\mu_0\right)\mu^{(r)}}{5\,\mu_0\left(3\,\kappa_0 + 4\,\mu_0\right)}\boldsymbol{\mathcal{K}} + \frac{3\,\kappa^{(r)} + 4\,\mu_0}{3\,\kappa_0 + 4\,\mu_0}\boldsymbol{\mathcal{J}}. \tag{2.37}$$

Then

$$\mathbf{E}^{(r)} = \left[\boldsymbol{\mathcal{I}} + \mathbf{P}^{(r)} : \left(\boldsymbol{\mathcal{L}}^{(r)} - \boldsymbol{\mathcal{L}}^{(0)}\right)\right]^{-1} =$$

$$= \frac{5\,\mu_0\left(3\,\kappa_0 + 4\,\mu_0\right)}{\mu_0\left(9\,\kappa_0 + 8\,\mu_0\right) + 6\left(\kappa_0 + 2\,\mu_0\right)\mu^{(r)}}\boldsymbol{\mathcal{K}} + \frac{3\,\kappa_0 + 4\,\mu_0}{3\,\kappa^{(r)} + 4\,\mu_0}\boldsymbol{\mathcal{J}}. \tag{2.38}$$

2.6.1 Incompressible phases

The "deformation rate concentration tensor" is (Kailasam and Ponte Castañeda, 1998, p. 436, eqn (14); Ponte Castañeda, 2005, p. 109; Ponte Castañeda, 1997, p. 146)

$$\mathbf{D}^{(r)} = \mathbf{A}^{(r)} : \mathbf{D}, \qquad \mathbf{A}^{(r)} = \mathbf{E}^{(r)} : \left(\sum_{s=1}^{N} c^{(s)}\,\mathbf{E}^{(s)}\right)^{-1}. \tag{2.39}$$

We have that

$$\sum_{s=1}^{N} c^{(s)}\, \mathbf{E}^{(s)} = \sum_{s=1}^{N} c^{(s)} \left[\frac{5\,\mu_0\,(3\,\kappa_0 + 4\,\mu_0)}{\mu_0\,(9\,\kappa_0 + 8\,\mu_0) + 6\,(\kappa_0 + 2\,\mu_0)\,\mu^{(s)}} \boldsymbol{\mathcal{K}} + \frac{3\,\kappa_0 + 4\,\mu_0}{3\,\kappa^{(s)} + 4\,\mu_0} \boldsymbol{\mathcal{J}} \right] =$$

$$= \left(\sum_{s=1}^{N} c^{(s)} \frac{3\,\kappa_0 + 4\,\mu_0}{3\,\kappa^{(s)}} + 4\,\mu_0 \right) \boldsymbol{\mathcal{J}} + \left[\sum_{s=1}^{N} \frac{5\,c^{(s)}\,\mu_0\,(3\,\kappa_0 + 4\,\mu_0)}{\mu_0\,(9\,\kappa_0 + 8\,\mu_0) + 6\,(\kappa_0 + 2\,\mu_0)\,\mu^{(s)}} \right] \boldsymbol{\mathcal{K}}. \quad (2.40)$$

Then

$$\left(\sum_{s=1}^{N} c^{(s)}\, \mathbf{E}^{(s)} \right)^{-1} =$$

$$= \left(\sum_{s=1}^{N} c^{(s)} \frac{3\,\kappa_0 + 4\,\mu_0}{3\,\kappa^{(s)} + 4\,\mu_0} \right)^{-1} \boldsymbol{\mathcal{J}} + \left[\sum_{s=1}^{N} \frac{5\,c^{(s)}\,\mu_0\,(3\,\kappa_0 + 4\,\mu_0)}{\mu_0\,(9\,\kappa_0 + 8\,\mu_0) + 6\,(\kappa_0 + 2\,\mu_0)\,\mu^{(s)}} \right]^{-1} \boldsymbol{\mathcal{K}} \quad (2.41)$$

and

$$\mathbf{A}^{(r)} = \mathbf{E}^{(r)} : \left(\sum_{s=1}^{N} c^{(s)}\, \mathbf{E}^{(s)} \right)^{-1} = \frac{1}{3\,\kappa^{(r)} + 4\,\mu_0} \left(\sum_{s=1}^{N} \frac{c^{(s)}}{3\,\kappa^{(s)} + 4\,\mu_0} \right)^{-1} \boldsymbol{\mathcal{J}} +$$

$$+ \frac{5\,\mu_0\,(3\,\kappa_0 + 4\,\mu_0)}{\mu_0\,(9\,\kappa_0 + 8\,\mu_0) + 6\,(\kappa_0 + 2\,\mu_0)\,\mu^{(r)}} \left[\sum_{s=1}^{N} \frac{5\,c^{(s)}\,\mu_0\,(3\,\kappa_0 + 4\,\mu_0)}{\mu_0\,(9\,\kappa_0 + 8\,\mu_0) + 6\,(\kappa_0 + 2\,\mu_0)\,\mu^{(s)}} \right]^{-1} \boldsymbol{\mathcal{K}} \,. \quad (2.42)$$

If all phases involved are imcompressible, then $\kappa_0 = \kappa^{(r)} = \infty$ and $D_{kk} = D_{kk}^{(r)} = 0$. In that case

$$\mathbf{D}^{(r)} = \mathbf{A}^{(r)} : \mathbf{D} =$$

$$= \lim_{\kappa^{(0)} \to \infty} \frac{5\,\mu_0(3\,\kappa_0 + 4\,\mu_0)}{\mu_0(9\,\kappa_0 + 8\,\mu_0) + 6(\kappa_0 + 2\,\mu_0)\mu^{(r)}} \left[\sum_{s=1}^{N} \frac{5\,c^{(s)}\,\mu_0(3\,\kappa_0 + 4\,\mu_0)}{\mu_0(9\,\kappa_0 + 8\,\mu_0) + 6(\kappa_0 + 2\,\mu_0)\mu^{(s)}} \right]^{-1} \mathbf{D},$$

which leads to

$$\mathbf{D}^{(i)} = \alpha^{(i)}\, \mathbf{D}, \qquad \text{where} \qquad \alpha^{(i)} = \frac{y^{(i)}}{3\,y^{(i)} + 2\,y_0} \left(\sum_{s=1}^{N} \frac{c^{(s)}\,y^{(s)}}{3\,y^{(s)} + 2\,y_0} \right)^{-1} \,.$$

Then

$$\dot{\bar{\varepsilon}}^{(i)} = \alpha^{(i)} \left(c^{(r)}, y^{(r)} \right)\, \dot{\bar{\varepsilon}},$$

where

$$\dot{\bar{\varepsilon}}^{(i)} = \sqrt{\frac{2}{3}\, \mathbf{D}^{(i)} : \mathbf{D}^{(i)}} \qquad \text{(no sum on } i\text{)} \qquad \text{and} \qquad \dot{\bar{\varepsilon}} = \sqrt{\frac{2}{3}\, \mathbf{D} : \mathbf{D}} \,.$$

Note that

$$\alpha^{(i)} = \alpha^{(i)} \left(c^{(r)}, y^{(r)} \left(c^{(p)}, \sigma_0^{(p)} \right) \right) \,.$$

The variation of $\alpha^{(i)}$ with respect to $c^{(r)}$ and $\sigma_0^{(r)}$ is discussed in Appendix B.

2.7 Summary of constitutive equations

The constitutive model developed in the previous sections can be summarized as follows:

$$\mathbf{D} = \mathbf{D}^e + \mathbf{D}^p, \tag{2.43}$$

$$\mathbf{D}^e = \boldsymbol{\mathcal{M}}^e : \overset{\triangledown}{\boldsymbol{\sigma}}, \qquad \boldsymbol{\mathcal{M}}^e = \frac{1}{2\,G}\boldsymbol{\mathcal{K}} + \frac{1}{3\,\kappa}\boldsymbol{\mathcal{J}}, \tag{2.44}$$

$$\mathbf{D}^p = \dot{\bar{\varepsilon}}^p\,\mathbf{N}, \qquad \mathbf{N} = \frac{3}{2\,\sigma_e}\mathbf{s}, \tag{2.45}$$

$$\dot{\bar{\varepsilon}}^{p(i)} = \alpha^{(i)}\,\dot{\bar{\varepsilon}}^p, \qquad \alpha^{(i)} = \alpha^{(i)}\left(\bar{\varepsilon}^{p(k)}\right), \tag{2.46}$$

$$\Phi\left(\boldsymbol{\sigma}, \bar{\varepsilon}^{p(k)}\right) = \sigma_e - \bar{\sigma}_0\left(\bar{\varepsilon}^{p(k)}\right) = 0. \tag{2.47}$$

The plastic modulus H is defined as follows:

$$H\,\dot{\bar{\varepsilon}}^p \equiv -\sum_{k=1}^{N}\frac{\partial\Phi}{\partial\bar{\varepsilon}^{p(k)}}\dot{\bar{\varepsilon}}^{p(k)} = \sum_{k=1}^{N}\frac{\partial\bar{\sigma}_0}{\partial\bar{\varepsilon}^{p(k)}}\dot{\bar{\varepsilon}}^p\,\alpha^{(k)} = \dot{\bar{\varepsilon}}^p\sum_{k=1}^{N}\frac{\partial\bar{\sigma}_0}{\partial\sigma_0^{(k)}}\frac{\partial\sigma_0^{(k)}}{\partial\bar{\varepsilon}^{p(k)}}\alpha^{(k)} \tag{2.48}$$

so that

$$H = \sum_{k=1}^{N}\frac{\partial\bar{\sigma}_0}{\partial\sigma_0^{(k)}}h^{(k)}\,\alpha^{(k)},$$

where

$$h^{(k)} = \frac{d\sigma_0^{(k)}\left(\bar{\varepsilon}^{(k)}\right)}{d\bar{\varepsilon}^{(k)}} \qquad \text{(no sum on } k\text{)}$$

is the plastic modulus of phase k.

Chapter 3

Numerical implementation

3.1   Introduction

In this chapter, a methodology is developed for the numerical integration in the context of the finite element method of the constitutive equations resulting from the homogenization theory of an $N-$phase elastoplastic composite. The model presented in section 2 is valid for perfectly plastic phases. In the applications considered, hardening of the phases is accounted for in an approximate way: within each increment of the solution the phases are assumed to be perfectly plastic with a yield stress corresponding to the average equivalent plastic strain in each phases at the end of the increment $\bar{\varepsilon}_{n+1}^{p(i)}$. The value of $\bar{\varepsilon}_{n+1}^{p(i)}$ is one of the unknowns and is determined in the process of the numerical integration over the increment.

3.2   Numerical Integration of the Constitutive Equations

In a finite element environment, the solution is developed incrementally and the constitutive equations are integrated numerically at the element Gauss integration points. In a displacement based finite element formulation the solution is deformation driven. Let $\mathbf{F}$ denote the deformation gradient tensor. At a given Gauss point, the solution $(\mathbf{F}_n, \boldsymbol{\sigma}_n)$ at time t_n as well as the deformation gradient $\mathbf{F}_{n+1}$ at time $t_{n+1} = t_n + \Delta t$ are known and the problem is to determine $\boldsymbol{\sigma}_{n+1}$.

The time variation of the deformation gradient $\mathbf{F}$ during the time increment $[t_n, t_{n+1}]$ can be written as:

$$\mathbf{F}(t) = \Delta\mathbf{F}(t) \cdot \mathbf{F}_n = \mathbf{R}(t) \cdot \mathbf{U}(t) \cdot \mathbf{F}_n, \qquad t_n \leq t \leq t_{n+1}, \tag{3.1}$$

where $\mathbf{R}(t)$ and $\mathbf{U}(t)$ are the rotation and right stretch tensors associated with $\Delta\mathbf{F}(t)$. The corresponding deformation rate tensor $\mathbf{D}(t)$ can be written as:

$$\mathbf{D}(t) \equiv \left[\dot{\mathbf{F}}(t) \cdot \mathbf{F}^{-1}(t)\right]_s = \left[\Delta\dot{\mathbf{F}}(t) \cdot \Delta\mathbf{F}^{-1}(t)\right]_s, \tag{3.2}$$

where the subscripts s and a denote the symmetric and anti-symmetric parts, respectively. If it is assumed that the Lagrangian triad associated with $\Delta \mathbf{F}(t)$ (i.e., the eigenvectors of $\mathbf{U}(t)$) remains fixed over the time interval (t_n, t_{n+1}), it can be shown readily that

$$\mathbf{D}(t) = \mathbf{R}(t) \cdot \dot{\mathbf{E}}(t) \cdot \mathbf{R}^T(t), \quad \mathbf{W}(t) = \dot{\mathbf{R}}(t) \cdot \mathbf{R}^T(t), \tag{3.3}$$

and

$$\overset{\triangledown}{\boldsymbol{\sigma}}(t) = \mathbf{R}(t) \cdot \dot{\hat{\boldsymbol{\sigma}}}(t) \cdot \mathbf{R}^T(t) \tag{3.4}$$

where $\mathbf{E}(t) = \ln \mathbf{U}(t)$ is the logarithmic strain associated with the increment, and

$$\hat{\boldsymbol{\sigma}}(t) = \mathbf{R}^T(t) \cdot \boldsymbol{\sigma}(t) \cdot \mathbf{R}(t). \tag{3.5}$$

It is noted that at the start of the increment $(t = t_n)$

$$\Delta \mathbf{F}_n = \mathbf{R}_n = \mathbf{U}_n = \boldsymbol{\delta}, \qquad \hat{\boldsymbol{\sigma}}_n = \boldsymbol{\sigma}_n, \quad \text{and} \quad \mathbf{E}_n = \mathbf{0}, \tag{3.6}$$

whereas at the end of the increment $(t = t_{n+1})$

$$\Delta \mathbf{F}_{n+1} = \mathbf{F}_{n+1} \cdot \mathbf{F}_n^{-1} = \mathbf{R}_{n+1} \cdot \mathbf{U}_{n+1} = \text{known}, \quad \text{and} \quad \mathbf{E}_{n+1} = \ln \mathbf{U}_{n+1} = \text{known}. \tag{3.7}$$

Then, the constitutive equations summarized in section 2.7 can be written in the form

$$\dot{\mathbf{E}} = \dot{\mathbf{E}}^e + \dot{\mathbf{E}}^p, \tag{3.8}$$

$$\dot{\mathbf{E}}^e = \boldsymbol{\mathcal{M}} : \dot{\hat{\boldsymbol{\sigma}}} \qquad \text{or} \qquad \dot{\hat{\boldsymbol{\sigma}}} = \boldsymbol{\mathcal{L}}^e : \dot{\mathbf{E}}^e, \qquad \boldsymbol{\mathcal{L}}^e = 2\, G\, \boldsymbol{\mathcal{K}} + 3\, \kappa\, \boldsymbol{\mathcal{J}}, \tag{3.9}$$

$$\dot{\mathbf{E}}^p = \dot{\bar{\varepsilon}}^p\, \hat{\mathbf{N}}, \qquad \hat{\mathbf{N}} = \frac{3}{2\, \sigma_e} \hat{\mathbf{s}}, \qquad \sigma_e = \sqrt{\frac{3}{2} \hat{\mathbf{s}} : \hat{\mathbf{s}}}, \tag{3.10}$$

$$\dot{\bar{\varepsilon}}^{p(i)} = \alpha^{(i)}\, \dot{\bar{\varepsilon}}^p, \qquad \alpha^{(i)} = \alpha^{(i)} \left(\bar{\varepsilon}^{p(k)} \right), \tag{3.11}$$

$$\Phi \left(\hat{\boldsymbol{\sigma}}, \bar{\varepsilon}^{p(k)} \right) = \sigma_e - \bar{\sigma}_0 \left(\bar{\varepsilon}^{p(k)} \right) = 0. \tag{3.12}$$

Previous experience (Aravas and Ponte Castañeda, 2004) shows that it is essential to use a backward Euler scheme for the numerical integration of the "plastic flow" equation in order to be able to use increments of reasonable size (i.e., several times the flow strain), whereas either the forward or the backward Euler method can be used.

In the following, we use two different ways for the integration of the aforementioned constitutive equations. In the first, we use a combination of the backward and the forward Euler method; in the second, we use only the backward Euler method.

3.2.1 Integration using a combination of backward and the forward Euler schemes

Equations (3.8) and (3.9) are integrated exactly:

$$\Delta \mathbf{E} = \Delta \mathbf{E}^e + \Delta \mathbf{E}^p, \tag{3.13}$$

$$\hat{\boldsymbol{\sigma}}_{n+1} = \boldsymbol{\sigma}_n + \boldsymbol{\mathcal{L}}^e : \Delta \mathbf{E}^e = \boldsymbol{\sigma}_n + \boldsymbol{\mathcal{L}}^e : (\Delta \mathbf{E} - \Delta \mathbf{E}^p) = \hat{\boldsymbol{\sigma}}^e - \boldsymbol{\mathcal{L}}^e : \Delta \mathbf{E}^p, \tag{3.14}$$

where $\hat{\boldsymbol{\sigma}}^e = \boldsymbol{\sigma}_n + \boldsymbol{\mathcal{L}}^e : \Delta \mathbf{E}$ is the "elastic predictor" and the notation $\Delta A = A_{n+1} - A_n$ is used.

The plastic flow rule (3.10) is integrated using the backward Euler method:

$$\Delta \mathbf{E}^p = \Delta \bar{\varepsilon}^p \, \hat{\mathbf{N}}_{n+1}. \tag{3.15}$$

Then (3.14) becomes

$$\hat{\boldsymbol{\sigma}}_{n+1} = \hat{\boldsymbol{\sigma}}^e - 2\,G\,\Delta\bar{\varepsilon}^p\,\hat{\mathbf{N}}_{n+1}. \tag{3.16}$$

Last equation shows that $\hat{\mathbf{s}}_{n+1}$ is co-linear with $\hat{\boldsymbol{\sigma}}^e$. The proof is as follows. If we substitute the definition of $\hat{\mathbf{N}}$ from (3.9) into the deviatoric part of (3.16), we find that

$$\hat{\mathbf{s}}_{n+1} = \hat{\mathbf{s}}^e - \frac{3\,G\,\Delta\bar{\varepsilon}^p}{\sigma_e^e}\hat{\mathbf{s}}_{n+1} \qquad \text{or} \qquad \hat{\mathbf{s}}_{n+1} = \left(1 + \frac{3\,G\,\Delta\bar{\varepsilon}^p}{\sigma_e^e}\right)^{-1}\hat{\mathbf{s}}^e, \tag{3.17}$$

i.e., $\hat{\mathbf{s}}_{n+1}$ and $\hat{\mathbf{s}}^e$ are indeed co-linear. Then

$$\hat{\mathbf{N}}_{n+1} = \frac{3}{2\,\sigma_e|_{n+1}}\hat{\mathbf{s}}_{n+1} = \frac{3}{2\,\sigma_e^e}\mathbf{s}^e \equiv \hat{\mathbf{N}}^e = \text{known}. \tag{3.18}$$

We dot (3.16) with $\hat{\mathbf{N}}_{n+1} = \hat{\mathbf{N}}^e$:

$$\underbrace{\hat{\boldsymbol{\sigma}}_{n+1} : \hat{\mathbf{N}}_{n+1}}_{\sigma_e|_{n+1}} = \underbrace{\hat{\boldsymbol{\sigma}}^e : \hat{\mathbf{N}}^e}_{\sigma_e^e} - 2\,G\,\Delta\bar{\varepsilon}^p\,\underbrace{\hat{\mathbf{N}}_{n+1} : \hat{\mathbf{N}}_{n+1}}_{3/2}$$

so that

$$\sigma_e|_{n+1} = \sigma_e^e - 3\,G\,\Delta\bar{\varepsilon}^p. \tag{3.19}$$

Next, equations (3.11) are integrated with the *forward* Euler scheme:

$$\Delta\bar{\varepsilon}^{p(i)} = \Delta\bar{\varepsilon}^p\,\alpha_n^{(i)}, \qquad \alpha_n^{(i)} = \alpha^{(i)}\left(\bar{\varepsilon}_n^{p(k)}\right).$$

The yield condition is written in the form

$$\sigma_e|_{n+1} - \bar{\sigma}_0|_{n+1} = 0, \qquad \bar{\sigma}_0|_{n+1} = \bar{\sigma}_0\left(\bar{\varepsilon}_{n+1}^{p(i)}\right) = \bar{\sigma}_0\left(\bar{\varepsilon}_n^{p(i)} + \Delta\bar{\varepsilon}^p\,\alpha_n^{(i)}\right), \tag{3.20}$$

and, in view of (3.19), becomes an equation to be solved for $\Delta\bar{\varepsilon}^p$:

$$\Phi\left(\Delta\bar{\varepsilon}^p\right) \equiv \sigma_e^e - 3\,G\,\Delta\bar{\varepsilon}^p - \bar{\sigma}_0|_{n+1}\left(\Delta\bar{\varepsilon}^p\right) = 0. \tag{3.21}$$

Newton's method is used for the solution of (3.21). The Jacobian of the Newton loop is

$$\frac{\partial\Phi}{\partial\bar{\varepsilon}^p} = -3\,G - \sum_{k=1}^{N}\left(\frac{\partial\bar{\sigma}_0}{\partial\bar{\varepsilon}^{p(k)}}\frac{\partial\bar{\varepsilon}^{p(k)}}{\partial\bar{\varepsilon}^p}\right)_{n+1} = -3\,G - \sum_{k=1}^{N}\left(\frac{\partial\bar{\sigma}_0}{\partial\bar{\varepsilon}^{p(k)}}\right)_{n+1}\alpha_n^{(i)}. \tag{3.22}$$

Also

$$\frac{\partial\bar{\sigma}_0}{\partial\bar{\varepsilon}^{p(k)}} = \frac{\partial\bar{\sigma}_0}{\partial\sigma_0^{(k)}}\frac{\partial\sigma_0^{(k)}}{\partial\bar{\varepsilon}^{p(k)}} = \frac{\partial\bar{\sigma}_0}{\partial\sigma_0^{(k)}}h^{(k)},$$

so that $(3.22) \Rightarrow$

$$\frac{\partial \Phi}{\partial \bar{\varepsilon}^p} = -3\,G - \sum_{k=1}^{N} \left(\frac{\partial \bar{\sigma}_0}{\partial \sigma_0^{(k)}} \right)_{n+1} h_{n+1}^{(k)}\, \alpha_n^{(i)}.$$

A first estimate for $\bar{\sigma}_0|_{n+1}\left(\Delta \bar{\varepsilon}^p\right)$ in the Newton iterations is determined as follows:

$$\bar{\sigma}_0|_{n+1}\left(\Delta \bar{\varepsilon}^p\right) = \bar{\sigma}_0 \left(\bar{\varepsilon}_{n+1}^{p(k)}\left(\Delta \bar{\varepsilon}^p\right) \right) \simeq \bar{\sigma}_0|_n + \sum_{k=1}^{N} \left(\frac{\partial \bar{\sigma}_0}{\partial \bar{\varepsilon}^{p(k)}} \frac{\partial \bar{\varepsilon}^{p(k)}}{\partial \bar{\varepsilon}^p} \right)_n \Delta \bar{\varepsilon}^p =$$

$$= \bar{\sigma}_0|_n + \sum_{k=1}^{N} \left(\frac{\partial \bar{\sigma}_0}{\partial \sigma_0^{(k)}}\, h^{(k)}\, \alpha^{(k)} \right)_n \Delta \bar{\varepsilon}^p = \bar{\sigma}_0|_n + H_n\, \Delta \bar{\varepsilon}^p, \qquad (3.23)$$

so that (3.21) becomes

$$\Phi\left(\Delta \bar{\varepsilon}^p\right) \simeq \sigma_e^e - 3\,G\,\Delta \bar{\varepsilon}^p - \bar{\sigma}_0|_n - H_n\, \Delta \bar{\varepsilon}^p = 0 \qquad \Rightarrow \qquad \Delta \bar{\varepsilon}^p = \frac{\sigma_e^e - \bar{\sigma}_0|_n}{3\,G + H_n}.$$

Finally, $\hat{\boldsymbol{\sigma}}_{n+1}$ is computed from (3.16) and the integration is completed with the transformation

$$\boldsymbol{\sigma}_{n+1} = \mathbf{R}_{n+1} \cdot \hat{\boldsymbol{\sigma}}_{n+1} \cdot \mathbf{R}_{n+1}^T. \qquad (3.24)$$

3.2.2 Integration using the backward Euler method on all variables

We recall equation (3.19):

$$\sigma_e|_{n+1} = \sigma_e^e - 3\,G\,\Delta \bar{\varepsilon}^p,$$

and use a *backward* Euler scheme for the numerical integration of (3.11):

$$\Delta \bar{\varepsilon}^{p(i)} = \Delta \bar{\varepsilon}^p\, \alpha^{(i)} \left(\bar{\varepsilon}_n^{p(k)} + \Delta \bar{\varepsilon}^{p(k)} \right). \qquad (3.25)$$

The yield condition now becomes

$$\sigma_e^e - 3\,G\,\Delta \bar{\varepsilon}^p - \bar{\sigma}_0 \left(\bar{\varepsilon}_n^{p(k)} + \Delta \bar{\varepsilon}^{p(k)} \right) = 0. \qquad (3.26)$$

Equations (3.25) and (3.26) is now a sytem of non-linear equations that needs to be solved for $\Delta \bar{\varepsilon}^p$ and $\Delta \bar{\varepsilon}^{(i)}$.

We choose $\Delta \bar{\varepsilon}^p$ as the primary unknown and treat (3.26) as the basic equation, in which $\Delta \bar{\varepsilon}^{(i)}$ are defined by equations (3.25) in terms of $\Delta \bar{\varepsilon}^p$. In the process of solving (3.26) and for a given value of $\Delta \bar{\varepsilon}^p$, a local Newton loop is used for the solution of (3.25) for $\Delta \bar{\varepsilon}^{(i)}$.

Solution of equations (3.25) for given $\Delta \bar{\varepsilon}^{p(i)}$

We write (3.25) in the form

$$P_i \equiv \Delta \bar{\varepsilon}^{p(i)} - \Delta \bar{\varepsilon}^p\, \alpha^{(i)} \left(\bar{\varepsilon}_n^{p(k)} + \Delta \bar{\varepsilon}^{p(k)} \right) = 0. \qquad (3.27)$$

Newton's method is used for the solution of (3.27). The Jacobian for Newton loop is given by the equation:

$$\frac{\partial P_i{}^{p(j)}}{\partial \Delta \bar{\varepsilon}} = \delta_{ij} - \Delta \bar{\varepsilon}^p \left.\frac{\partial \alpha^{(i)}}{\partial \sigma_0^{(j)}}\right|_{n+1} h_{n+1}^{(j)}. \tag{3.28}$$

Solution of yield condition (3.26) for given $\Delta \bar{\varepsilon}^p$

The yield condition is written in the form

$$\Phi\left(\Delta \bar{\varepsilon}^p\right) \equiv \sigma_e^e - 3\,G\,\Delta \bar{\varepsilon}^p - \left.\bar{\sigma}_0\right|_{n+1}\left(\Delta \bar{\varepsilon}^p\right) = 0. \tag{3.29}$$

and is solved by using Newton's method. The Jacobian for Newton loop is given by the equation:

$$\frac{\partial \Phi}{\partial \Delta \bar{\varepsilon}^p} = -3\,G - \sum_{j=1}^{N}\left(\frac{\partial \bar{\sigma}_0}{\partial \Delta \bar{\varepsilon}^{p(j)}}\frac{\partial \Delta \bar{\varepsilon}^{p(j)}}{\partial \Delta \bar{\varepsilon}^p}\right)_{n+1}, \tag{3.30}$$

where

$$\frac{\partial \bar{\sigma}_0}{\partial \Delta \bar{\varepsilon}^{p(j)}} = \frac{\partial \bar{\sigma}_0}{\partial \bar{\varepsilon}^{p(j)}} = \frac{\partial \bar{\sigma}_0}{\partial \sigma_0^{(j)}}\frac{\partial \sigma_0^{(j)}}{\partial \bar{\varepsilon}^{p(j)}} = \frac{\partial \bar{\sigma}_0}{\partial \sigma_0^{(j)}}h^{(j)},$$

so that (3.30) becomes

$$\frac{\partial \Phi}{\partial \bar{\varepsilon}^p} = -3\,G - \sum_{j=1}^{N}\left(\frac{\partial \bar{\sigma}_0}{\partial \sigma_0^{(j)}}h^{(j)}\frac{\partial \bar{\varepsilon}^{p(j)}}{\partial \bar{\varepsilon}^p}\right)_{n+1}.$$

The derivatives $\frac{\partial \bar{\varepsilon}^{p(j)}}{\partial \bar{\varepsilon}^p}$ are determined from (3.27) as follows:

$$\frac{\partial \Delta \bar{\varepsilon}^{p(i)}}{\partial \Delta \bar{\varepsilon}^p} - \alpha_{n+1}^{(i)} - \Delta \bar{\varepsilon}^p \sum_{j=1}^{n}\left(\frac{\partial \alpha^{(i)}}{\partial \Delta \bar{\varepsilon}^{p(j)}}\frac{\partial \Delta \bar{\varepsilon}^{p(j)}}{\partial \Delta \bar{\varepsilon}^p}\right)_{n+1} = 0 \qquad \Rightarrow$$

$$\frac{\partial \Delta \bar{\varepsilon}^{p(i)}}{\partial \Delta \bar{\varepsilon}^p} - \alpha_{n+1}^{(i)} - \Delta \bar{\varepsilon}^p \sum_{j=1}^{n}\left(\frac{\partial \alpha^{(i)}}{\partial \sigma_0^{(j)}}h^{(j)}\frac{\partial \Delta \bar{\varepsilon}^{p(j)}}{\partial \Delta \bar{\varepsilon}^p}\right)_{n+1} = 0 \qquad \Rightarrow$$

$$\sum_{j=1}^{n}\left[\delta_{ij} - \Delta \bar{\varepsilon}^p\left(\frac{\partial \alpha^{(i)}}{\partial \sigma_0^{(j)}}h^{(j)}\right)_{n+1}\right]\frac{\partial \bar{\varepsilon}^{p(j)}}{\partial \bar{\varepsilon}^p} = \alpha_{n+1}^{(i)}. \tag{3.31}$$

The last equations provide a system of linear equations that is solved for $\frac{\partial \bar{\varepsilon}^{p(i)}}{\partial \bar{\varepsilon}^p}$.

3.3 The linearization moduli

The so-called "linearization moduli" C_{ijkl} are required, when the finite element method is used for the solution to the problem. They are defined as follows

$$C_{ijkl} \simeq \left.R_{im}\right|_{n+1}\left.R_{jn}\right|_{n+1}\left.R_{kp}\right|_{n+1}\left.R_{lq}\right|_{n+1}\hat{C}_{mnpq}, \qquad \text{where} \qquad \hat{\mathbf{C}} = \frac{\partial \hat{\boldsymbol{\sigma}}_{n+1}}{\partial \mathbf{E}_{n+1}}. \tag{3.32}$$

In general, $\mathbf{C}$ depends on both the constitutive model and the algorithm used for the numerical integration of the constitutive equations. The equation that defines $\hat{\boldsymbol{\sigma}}_{n+1}$ is

$$\hat{\boldsymbol{\sigma}}_{n+1} = \boldsymbol{\sigma}_n + \boldsymbol{\mathcal{L}}^e : \Delta\mathbf{E} - 2\,G\,\Delta\bar{\varepsilon}^p\,\hat{\mathbf{N}}^e \tag{3.33}$$

so that

$$d\hat{\boldsymbol{\sigma}}_{n+1} = \boldsymbol{\mathcal{L}}^e : d\mathbf{E}_{n+1} - 2\,G\,\left(d\bar{\varepsilon}^p\,\hat{\mathbf{N}}^e + \Delta\bar{\varepsilon}^p\,d\hat{\mathbf{N}}^e\right), \tag{3.34}$$

where

$$d\hat{\mathbf{N}}^e = \frac{2\,G}{\sigma_e^e}\left(\frac{3}{2}\boldsymbol{\mathcal{K}} - \hat{\mathbf{N}}^e\,\hat{\mathbf{N}}^e\right) : d\mathbf{E}_{n+1}.$$

The yield condition

$$\sigma_e|_{n+1} - \bar{\sigma}_0|_{n+1} = 0 \tag{3.35}$$

is used together with (3.34) for the determination of $d\hat{\boldsymbol{\sigma}}_{n+1}$ in terms of $d\mathbf{E}_{n+1}$ as follows. Equation (3.35) yields

$$0 = \underbrace{\frac{\partial\sigma_e|_{n+1}}{\partial\hat{\boldsymbol{\sigma}}_{n+1}}}_{\hat{\mathbf{N}}_{n+1}} = \hat{\mathbf{N}}^e : d\boldsymbol{\sigma}_{n+1} - \sum_{k=1}^{N}\left.\frac{\partial\bar{\sigma}_0}{\partial\bar{\varepsilon}^{p(k)}}\right|_{n+1}d\bar{\varepsilon}^{p(k)} =$$

$$= \hat{\mathbf{N}}^e : \left[\boldsymbol{\mathcal{L}}^e : d\boldsymbol{\varepsilon} - 2\,G\left(d\bar{\varepsilon}^p\,\hat{\mathbf{N}}^e + \Delta\bar{\varepsilon}^p\,d\hat{\mathbf{N}}^e\right)\right] - \sum_{k=1}^{N}\left.\frac{\partial\bar{\sigma}_0}{\partial\sigma_0^{(k)}}\right|_{n+1}h_{n+1}^{(k)}\,\alpha_n^{(i)}\,d\bar{\varepsilon}^p =$$

$$= \underbrace{\hat{\mathbf{N}}^e : \boldsymbol{\mathcal{L}}^e}_{2\,G\,\hat{\mathbf{N}}^e} : d\mathbf{E}_{n+1} - 2\,G\left(d\bar{\varepsilon}^p\,\underbrace{\hat{\mathbf{N}}^e : \hat{\mathbf{N}}^e}_{3/2} + \Delta\bar{\varepsilon}^p\,\underbrace{\hat{\mathbf{N}}^e : d\hat{\mathbf{N}}^e}_{0}\right) -$$

$$- \underbrace{\sum_{k=1}^{N}\left(\left.\frac{\partial\bar{\sigma}_0}{\partial\sigma_0^{(k)}}\right|_{n+1}h_{n+1}^{(k)}\,\alpha_n^{(i)}\right)}_{H_{n+1}}d\bar{\varepsilon}^p =$$

$$= 2\,G\,\hat{\mathbf{N}}^e : d\mathbf{E}_{n+1} - (3\,G + H_{n+1})\,d\bar{\varepsilon}^p, \tag{3.36}$$

so that

$$d\bar{\varepsilon}^p = \frac{2\,G}{3\,G + H_{n+1}}\,\hat{\mathbf{N}}^e : d\boldsymbol{\varepsilon}_{n+1}.$$

Then (3.34) implies

$$d\hat{\boldsymbol{\sigma}}_{n+1} = \boldsymbol{\mathcal{L}}^e : d\mathbf{E}_{n+1} - 2\,G\left[\frac{2\,G}{3\,G + H_{n+1}}\left(\hat{\mathbf{N}}^e : d\mathbf{E}_{n+1}\right)\hat{\mathbf{N}}^e + \right.$$

$$\left. + \Delta\bar{\varepsilon}^p\frac{2\,G}{\sigma_e^e}\left(\frac{3}{2}\boldsymbol{\mathcal{K}} - \hat{\mathbf{N}}^e\,\hat{\mathbf{N}}^e\right) : d\mathbf{E}_{n+1}\right] =$$

$$= \left\{\boldsymbol{\mathcal{L}}^e - 4\,G\left[\frac{1}{3 + \frac{H_{n+1}}{G}}\hat{\mathbf{N}}^e\,\hat{\mathbf{N}}^e + \Delta\bar{\varepsilon}^p\frac{G}{\sigma_e^e}\left(\frac{3}{2}\boldsymbol{\mathcal{K}} - \hat{\mathbf{N}}^e\,\hat{\mathbf{N}}^e\right)\right]\right\} : d\mathbf{E}_{n+1} =$$

$$= \left\{\boldsymbol{\mathcal{L}}^e - 4\,G\left(\frac{1}{3 + \frac{H_{n+1}}{G}} - \Delta\bar{\varepsilon}^p\frac{G}{\sigma_e^e}\right)\hat{\mathbf{N}}^e\,\hat{\mathbf{N}}^e - 6\,G\,\Delta\bar{\varepsilon}^p\frac{G}{\sigma_e^e}\boldsymbol{\mathcal{K}}\right\} : d\mathbf{E}_{n+1}, \tag{3.37}$$

so that

$$\hat{\mathbf{C}} = \boldsymbol{\mathcal{L}}^e - 4\,G\left(\frac{1}{3 + \frac{H_{n+1}}{G}} - \Delta\bar{\varepsilon}^p\frac{G}{\sigma_e^e}\right)\hat{\mathbf{N}}_{n+1}\,\hat{\mathbf{N}}_{n+1} - 6\,G\,\Delta\bar{\varepsilon}^p\frac{G}{\sigma_e^e}\boldsymbol{\mathcal{K}}. \tag{3.38}$$

Finally, (3.32) yields

$$\mathbf{C} \simeq \boldsymbol{\mathcal{L}}^e - 4\,G\left(\frac{1}{3 + \frac{H_{n+1}}{G}} - \Delta\bar{\varepsilon}^p\frac{G}{\sigma_e^e}\right)\mathbf{N}_{n+1}\,\mathbf{N}_{n+1} - 6\,G\,\Delta\bar{\varepsilon}^p\frac{G}{\sigma_e^e}\boldsymbol{\mathcal{K}}. \tag{3.39}$$

3.4 The role of UMAT(User MATerial subroutine)

The constitutive model for elastoplastic materials is implemented into the ABAQUS general purpose finite element code. This code provides a general interface so that a particular constitutive model can be introduced via a "user subroutine" named UMAT (User MATerial). The subroutine UMAT passes in all the information at the start of the increment, i.e., $\mathbf{F}_n$, $\boldsymbol{\sigma}_n$, $\bar{\varepsilon}_n^{p(r)}$, as well as $\mathbf{F}_{n+1}$ and the user has to calculate the values of the corresponding quantities at the end of the increment, i.e., $\boldsymbol{\sigma}_{n+1}$, and $\bar{\varepsilon}_{n+1}^{p(r)}$. The "linearization moduli" are also calculated in UMAT.

3.5 Integral formulation of the problem-The "weak" solution

In this section we present a brief description of the finite element formulation of the problem. We consider the spatial configuration of a general deformable body of initial volume V_0 at time $t = 0$. At time t the body is deformed to a volume V surrounded by a surface as shown in Figure 3.1. The body is loaded by body forces $\mathbf{b}$ per unit mass and traction forces $\mathbf{T}$ per unit area on the part S_σ of S, and imposed displacements $\hat{\mathbf{u}}$ on the remainder of S_u of S.

The equations of equilibrium are

$$\frac{\partial \sigma_{ij}}{\partial x_j} + \rho b_i = 0 \tag{3.40}$$

where σ_{ij} is the Cauchy stress tensor, and ρ is the mass density. The problem is completed by the kinematical relationships

$$D_{ij} = \frac{1}{2}\left(\frac{\partial \upsilon_i}{\partial x_j} + \frac{\partial \upsilon_j}{\partial x_i}\right) \tag{3.41}$$

where υ is the velocity field.
We consider that the displacement vector $\mathbf{u}$ is known on part of the boundary S_u:

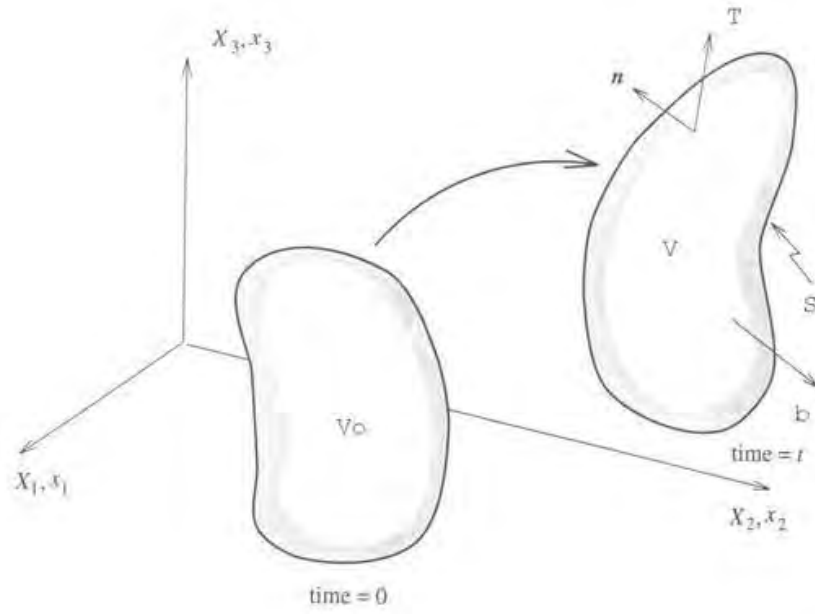$$\mathbf{u} = \hat{\mathbf{u}} \equiv \text{known on } S_u \tag{3.42}$$

Figure 3.1: Body deformation

On the remaining boundary S_σ the applied tractions are known:

$$\mathbf{n} \cdot \boldsymbol{\sigma} = \mathbf{T} \equiv \text{known on } S_\sigma \tag{3.43}$$

The problem can be formulated in an integral form as follows:

Find a displacement field $\mathbf{u} \in H^2$ such that $\mathbf{u} = \hat{\mathbf{u}}$ on S_u and

$$\int_V \left[\frac{\partial \sigma_{ij}(\mathbf{u})}{\partial x_j} + \rho b_i \right] u_i^* dV + \int_{S_\sigma} [n_j \, \sigma_{ij}(\mathbf{u}) - T_i] \, v_i^* dS = 0 \quad \forall \, \mathbf{u}^* \in H^0, \boldsymbol{v}^* \in H^0, \mathbf{u}^* = \mathbf{0} \text{ on } S_u \tag{3.44}$$

Then

$$\int_V \left[\frac{\partial \sigma_{ij}(\mathbf{u})}{\partial x_j} + \rho \, b_i \right] u_i^* \, dV = \int_V \frac{\partial \sigma_{ij}(\mathbf{u})}{\partial x_j} u_i^* \, dV + \int_V \rho \, b_i \, u_i^* \, dV =$$

$$= \int_V \left\{ \frac{\partial [\sigma_{ij}(\mathbf{u}) \, u_i^*]}{\partial x_j} - \sigma_{ij}(\mathbf{u}) \frac{\partial u_i^*}{\partial x_j} \right\} dV + \int_V \rho \, b_i \, u_i^* \, dV =$$

$$= \int_S \sigma_{ij}(\mathbf{u}) \, u_i^* \, n_j \, dS - \int_V \sigma_{ij}(\mathbf{u}) \, D_{ij}^* \, dV + \int_V \rho \, b_i \, u_i^* \, dV =$$

$$= \int_{S_u} \sigma_{ij}(\mathbf{u}) \, n_j \, \underbrace{u_i^*}_{0} \, dS + \int_{S_\sigma} \sigma_{ij}(\mathbf{u}) \, n_j \, u_i^* \, dS - \int_V \sigma_{ij}(\mathbf{u}) \, D_{ij}^* \, dV + \int_V \rho \, b_i \, u_i^* \, dV =$$

$$= \int_{S_\sigma} \sigma_{ij}(\mathbf{u}) \, n_j \, u_i^* \, dS - \int_V \sigma_{ij}(\mathbf{u}) \, D_{ij}^* + \int_V \rho \, b_i \, u_i^* \, dV. \tag{3.45}$$

We substitute in (3.44) to find

$$\int\limits_{S_\sigma} \sigma_{ij}\left(\mathbf{u}\right) n_j u_i^* \, dS - \int\limits_V \sigma_{ij}\left(\mathbf{u}\right) D_{ij}^* \, dV + \int\limits_V \rho \, b_i \, u_i^* \, dV + \int\limits_{S_\sigma} n_j \, \sigma_{ij}\left(\mathbf{u}\right) v_i^* \, dS - \int\limits_{S_\sigma} T_i \, v_i^* \, dS = 0$$

$$\forall \, \mathbf{u}^*, \boldsymbol{v}^* \in H. \quad (3.46)$$

In order to simplify the above expression, we choose $\mathbf{u}^* = -\boldsymbol{v}^*$. Then the problem becomes as follows:

Find a displacement field $\mathbf{u}\left(\mathbf{x}\right)$ such that $\mathbf{u} = \hat{\mathbf{u}}$ on S_u and

$$G\left(\mathbf{u}\left(\mathbf{x}\right)\right) \equiv \int\limits_V \boldsymbol{\sigma}\left(\mathbf{u}\left(\mathbf{x}\right)\right) : \mathbf{D}^* \, dV - \int\limits_V \rho \, \mathbf{b} \cdot \boldsymbol{v}^* \, dV - \int\limits_S \mathbf{T} \cdot \boldsymbol{v}^* \, dS = 0 \quad (3.47)$$

for all continuous and differentiable fields $\boldsymbol{v}^*\left(\mathbf{x}\right)$ that satisfy the condition $\boldsymbol{v}^* = \mathbf{0}$ on S_u . In the above equation

$$D_{ij}^* = \frac{1}{2}\left(\frac{\partial v_i^*}{\partial x_j} + \frac{\partial v_j^*}{\partial x_i}\right). \quad (3.48)$$

The vanishing of the non-linear functional $G\left(\mathbf{u}\right)$ for all "virtual" velocity fields $\boldsymbol{v}^*\left(\mathbf{x}\right)$ defines the "weak" solution $\mathbf{u}\left(\mathbf{x}\right)$ of the problem.

The integral statement (3.47) provides the basis for the finite element formulation as described in the following section.

3.6 Finite element formulation

In a finite element setting, the problem is solved incrementally and the primary unknown is the displacement increment $\Delta\mathbf{u}\left(\mathbf{x}\right)$ that defines the position of the body at the end of the increment:

$$\mathbf{u}_{n+1}\left(\mathbf{x}\right) = \mathbf{u}_n\left(\mathbf{x}\right) + \Delta\mathbf{u}\left(\mathbf{x}\right), \qquad \mathbf{x}_{n+1}\left(\mathbf{x}\right) = \mathbf{x}_n\left(\mathbf{x}\right) + \Delta\mathbf{u}\left(\mathbf{x}\right) = \mathbf{X} + \mathbf{u}_{n+1}\left(\mathbf{x}\right). \quad (3.49)$$

Next, we introduce the finite element interpolation, which, at the element level, can be written as

$$\left\{\Delta u\left(\mathbf{x}\right)\right\} = \left[N\left(\mathbf{x}\right)\right]\left\{\Delta u_e^N\right\} \quad (3.50)$$

where $\left[N\left(\mathbf{x}\right)\right]$ is the interpolation matrix, and $\left\{\Delta u_e^N\right\}$ the vector of nodal unknowns of the element. In the above equation and for the rest of this chapter, the following notation is used:

$$\left\{\ \right\} \text{ denotes a column}, \qquad \lfloor\ \rfloor \text{ denotes a row}, \qquad \left[\ \right] \text{ denotes a matrix}.$$

We can also write

$$\left\{D\left(\mathbf{x}\right)\right\} = \left[B\left(\mathbf{x}\right)\right]\left\{v_e^N\right\} \quad (3.51)$$
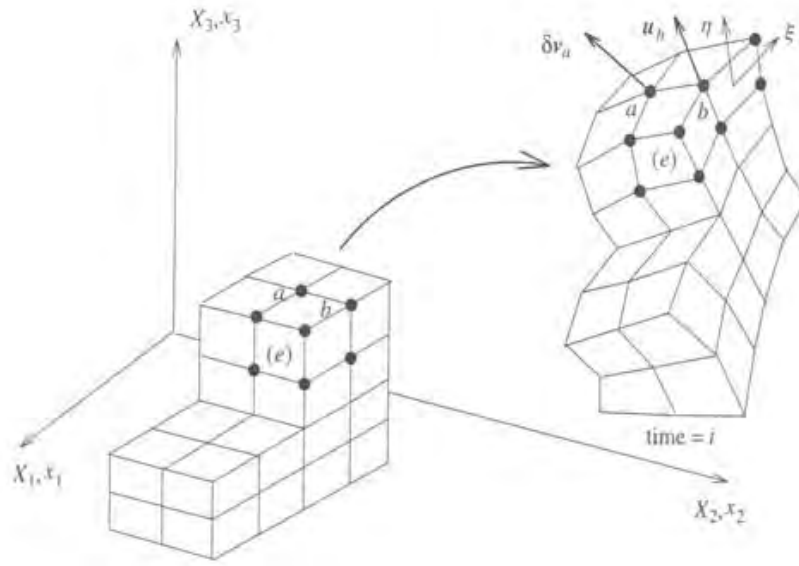
Figure 3.2: Discretization

Similarly

$$\{v^*(\mathbf{x})\} = [N(\mathbf{x})] \{v_e^{*N}\} \tag{3.52}$$

and

$$\{D^*(\mathbf{x})\} = [B(\mathbf{x})] \{v_e^{*N}\} \tag{3.53}$$

Substituting equations (3.52) and (3.53) in (3.47) we find

$$G = \lfloor v_e^{*N} \rfloor \underset{e}{\mathbf{A}} \left(\int\limits_{V_{n+1}^e} [B]_{n+1}^T \{\sigma\}_{n+1} \, dV - \int\limits_{V_{n+1}^e} \rho \, [N]_{n+1}^T \{b\}_{n+1} \, dV - \int\limits_{S_{\sigma\,n+1}^e} [N]_{n+1}^T \{T\}_{n+1} \, dS \right) = 0,$$

where $\underset{e}{\mathbf{A}}$ is the "assembly operator" Since last equation must hold for arbitrary values of $\lfloor v^{*N} \rfloor$, we have that

$$\underset{e}{\mathbf{A}} \left(\int\limits_{V_{n+1}^e} [B]_{n+1}^T \{\sigma\}_{n+1} \, dV - \int\limits_{V_{n+1}^e} \rho \, [N]_{n+1}^T \{b\}_{n+1} \, dV - \int\limits_{S_{\sigma\,n+1}^e} [N]_{n+1}^T \{T\}_{n+1} \, dS \right) = 0$$

or

$$\underset{e}{\mathbf{A}} \int\limits_{V_{n+1}^e} [B]_{n+1}^T \{\sigma\}_{n+1} \, dV = \{F\}_{n+1}, \tag{3.54}$$

where

$$\{F\}_{n+1} = \underset{e}{\mathbf{A}} \left(\int\limits_{V_{n+1}^e} [N]_{n+1}^T \rho \{b\}_{n+1} \, dV + \int\limits_{S_{\sigma\,n+1}^e} [N]_{n+1}^T \{T\}_{n+1} \, dS \right) \tag{3.55}$$

is the global vector of applied loads. The quantity $\{\sigma\}_{n+1}$ in (3.54) is a non-linear function of the unknown nodal displacement increments $\{\Delta u^N\}$. Equation (3.54) provides the set of non-linear equations that determine $\{\Delta u^N\}$. In fact, (3.54) can be written as

$$\left\{R\left(\Delta u^N\right)\right\}_{n+1} \equiv \mathbf{A}_e \int_{V_{n+1}^e} [B_L]_{n+1}^T \left\{\sigma\left(\Delta u^N\right)\right\}_{n+1} dV - \{F\}_{n+1} = \{0\}, \tag{3.56}$$

where $\left\{R\left(\Delta u^N\right)\right\}_{n+1}$ is the global residual force vector, i.e., the difference between the forces required to maintain $\{\sigma\}_{n+1}$ in the body and the applied forces $\{F\}_{n+1}$.

The non-linear system (3.56) is solved for $\{\Delta u^N\}$ by using Newton's method. The corresponding Jacobian matrix, which plays the role of the "stiffness matrix" now, is determined by using (3.6) as follows. We write (3.6) in the form

$$G = \lfloor v^{*N} \rfloor \{R\}_{n+1} = 0 \tag{3.57}$$

and calculate

$$dG = \lfloor v^{*N} \rfloor \frac{\partial \left\{R\left(\Delta u^N\right)\right\}_{n+1}}{\partial \{\Delta u^N\}} d\{\Delta u^N\} = \lfloor v^{*N} \rfloor [J] d\{\Delta u^N\} = 0, \tag{3.58}$$

where $[J]$ now is the required Jacobian.

Chapter 4

Unit cell calculations

4.1 Introduction

In this chapter we consider a two-phase steel made of an austenitic matrix that contains dispersed martensite and the homogenization technique is used to determine the overall behavior of the two-phase steel. The corresponding "unit cell" for the two-phase steel is also defined. Then, unit cell calculations for the corresponding problem of uniaxial tension are carried out and the results are compared with those of the homogenization theory.

4.2 Modeling the microstructure of the two-phase steel

The two-phase composite we examine consists of particles of martensite isotropically and homogeneously dispersed in the matrix phase of austenite. The microstructure of the composite material can be described approximately by a three-dimensional periodic array of identical prismatic cells. Every cell models the two phases of the composite and consists of a martensitic spherical inclusion embedded in the center of a hexagonal prism simulating the austenitic matrix. Figure 4.1 shows a schematic representation of the three-dimensional periodic array of prismatic cells. The periodic array of prismatic cells shown in Figure 4.1 is extended in all three directions. In order to minimize the calculations, we replace the prismatic cells with the corresponding cylindrical cells as shown in Figures 4.2 and 4.3.
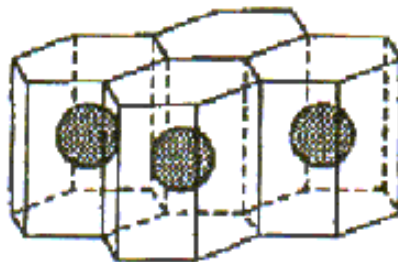
Figure 4.1: Three-dimensional periodic array of prismatic cells
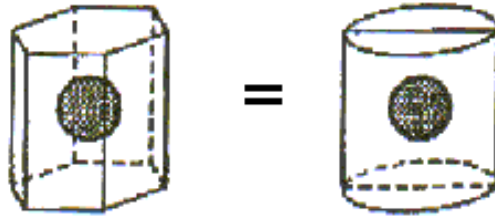
Figure 4.2: Prismatic cell approximated by cylindrical cell

4.3 The unit cell problem — uniaxial tension

In this section we use the ABAQUS general purpose finite element program in order to solve the corresponding cylindrical unit cell problem with the appropriate periodic boundary conditions for the problem of uniaxial tension.

The spherical inclusion embedded in the center of the cylinder shown in Figure 4.3 models the martensitic particles and its radius R is related with the volume fraction of martensite f according to the equation:

$$f = \frac{V_{mart}}{V_{total}} = \frac{V_{sphere}}{V_{total}} = \frac{\frac{4}{3}\pi R^3}{\pi R_c^2 h} \qquad \Rightarrow \qquad R = \left(\frac{3}{4} f R_c^2 h\right)^{1/3} \tag{4.1}$$

where R_c is the radius of the cylindrical cell and h its height. The height h is assumed equal to $2R_c$, so that the last equation implies that

$$\frac{R}{R_c} = \left(\frac{3}{2} f\right)^{1/3}. \tag{4.2}$$
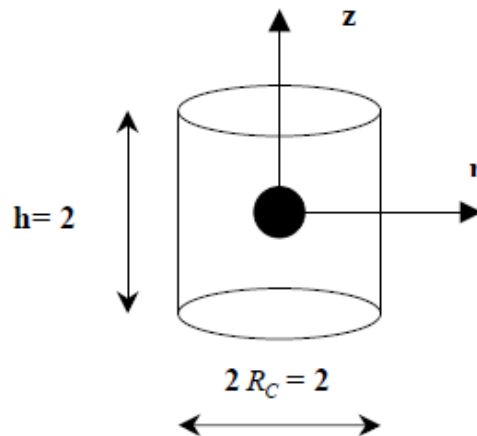
Figure 4.3: Dimensions of the cylindrical cell

The axisymmetric problem is symmetric about the midplane at $z = 0$; therefore we need to model one-quarter of the cross-section on the $z - r$ plane as shown in Figure 4.4, where the dark area represents the martensitic phase.

A typical finite element mesh used in the calculations is shown in Figure 4.5.
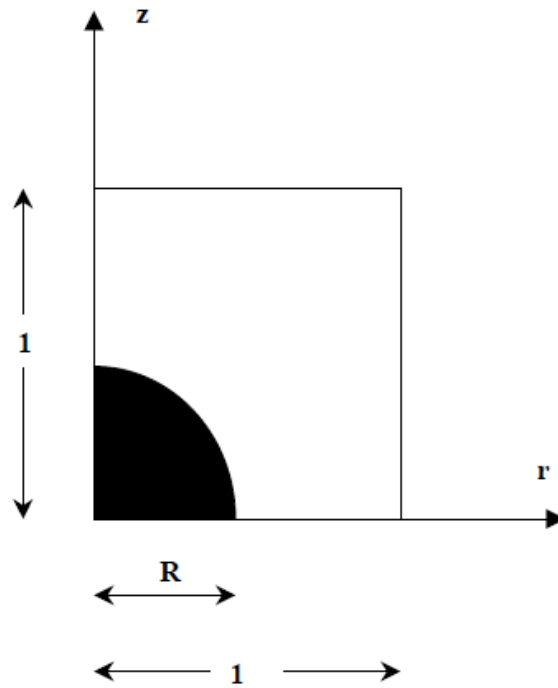
Figure 4.4: FEM modeling of Unit Cell
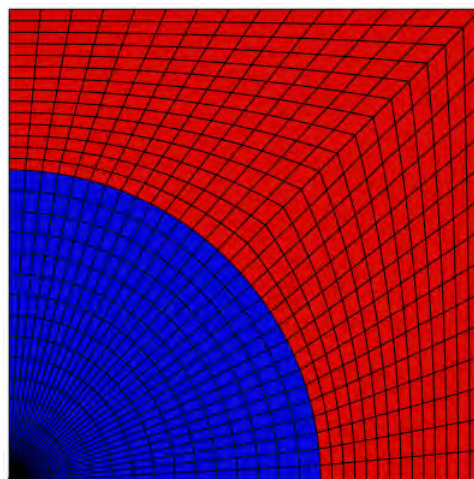
Figure 4.5: Finite element mesh that corresponds to the case with $f = 0.20$, i.e., 20% of martensite volume. The blue elements correspond to the martensitic particles and the red elements are the austenitic matrix.

Figure 4.6 shows schematically the aforementioned successive geometric approximations involved in the modeling, i.e., the steps that lead form the actual three-dimensional prismatic unit cells to the axisymmetric finite element modeling of the unit cell.
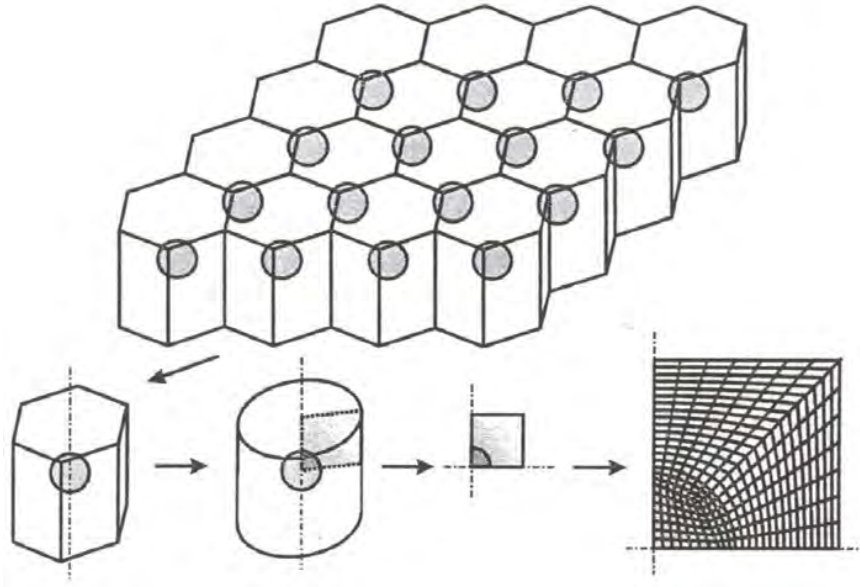
Figure 4.6: Schematic depiction of the idea of unit cell modeling.

Five different volume fractions are analyzed, namely $f = 0.10, 0.20, 0.30, 0.40, 0.50$. The corresponding values of the ratio R/R_c are shown in Table 4.1.

Table 4.1:
f and R/R_c for the FEM models examined

MODEL	f(%)	R/R_c
I	10	0.531
II	20	0.660
III	30	0.766
IV	40	0.840
V	50	0.908

4.4   Boundary conditions

The finite element used in the calculations are four-node axisymmetric, isoparametric "B-bar" elements (CAX4H in ABAQUS). A "finite strain" analysis is carried out. In order to

model a uniaxial tension test, we impose a uniform displacement on the top side of the mesh until a final elongation of 20% is reached.

Boundary conditions along the other three sides of the model provide the necessary symmetry and periodicity conditions for modeling the infinite series of stacked cells in uniaxial tension. All nodes along the midplane are constrained to move only in the radial direction, and all nodes along the pole (z-axis) are constrained to have zero radial displacement. Also, all nodes on the outer edge of the cell are constrained to have equal radial displacements. A schematic representation of the boundary conditions is shown in Figure 4.7.
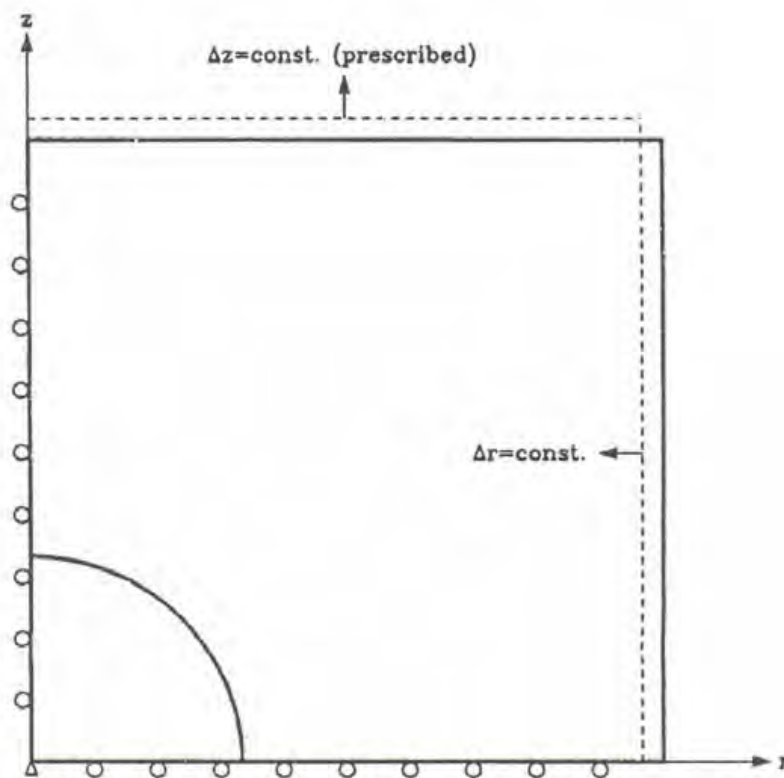
Figure 4.7: Schematic description of the problem with the boundary conditions.

4.5 Hardening of the phases

The two phases involved (austenite and martensite) are modeled as elastic-plastic materials that obey the classical von Mises yield criterion with the associated flow rule. The hardening behavior of martensite was obtained from experimental data of the partly martensitic steel DOCOL 1400 (volume fraction of martensite 95%) presented in Technical steel research (2002) and of austenite from experimental data of Naturani et al. (1982). The hardening behavior of the two phases is described by the following equations

$$\text{austenite:} \quad \sigma_y^{(\alpha)}\left(\bar{\varepsilon}^{p(a)}\right) = 300 + 500\left(\bar{\varepsilon}^{p(a)}\right)^{0.25} \text{(MPa)} \tag{4.3}$$

$$\text{martensite:} \quad \sigma_y^{(m)}\left(\bar{\varepsilon}^{p(m)}\right) = 1200 + 1025\left(\bar{\varepsilon}^{p(m)}\right)^{0.25} \text{(MPa)}, \tag{4.4}$$

where the superscripts (α) and (m) denote austenite and martensite respectively.

4.6 Comparison of the predictions of the homogenization theory with the unit cell calculations

The unit cell problem is solved with ABAQUS for the five cases shown in Table 4.1. The deformed finite element meshes at the final elongation of 20% are shown in Figure 4.13.

The homogenization method described in Chapter 2 is also used for the analysis of the problem of uniaxial tension of the homogenized two-phase composite. We consider both the Hashin-Shtrikman $\left(\mu_0 = \mu^{(1)}\right)$ and the Reuss model $\left(\frac{1}{\mu_0} = \sum\limits_{r=1}^{N} \frac{c^{(r)}}{\mu^{(r)}}\right)$ for the calculation of the reference modulus μ_0.

A value of $E = 200$ GPa and $\nu = 0.3$ for Young's modulus and Poisson ratio respectively are used in the calculations for both the austenite and the martensite.

The results of the three methods are compared in Figures 4.8-4.12. It is found that the predictions of the three methods agree reasonably well in the first two cases with $f = 10\%$ and $f = 20\%$. But, as the volume fraction of the martensite increases beyond 30%, we observe that the predictions differ with the Reuss model being closer to the unit cell.

Figures 4.14-4.18 show contours of the equivalent plastic strain $\bar{\varepsilon}^p$ in the unit cells for various volume fractions of martensite.
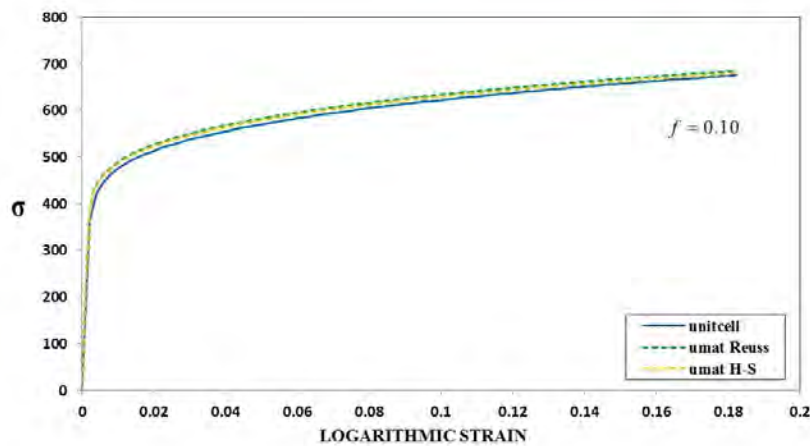
- **Model I (f=10%)**

Figure 4.8: Comparison of stress-strain curves for f =10%.

- **Model II (f=20%)**
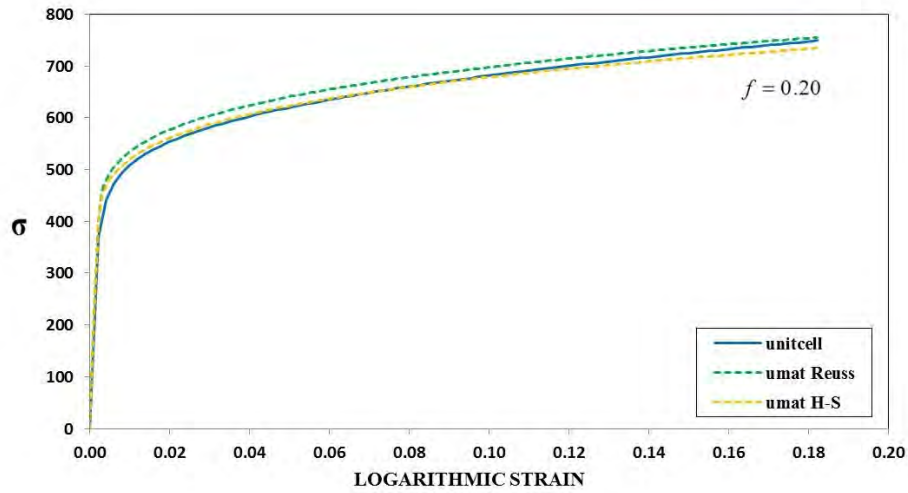

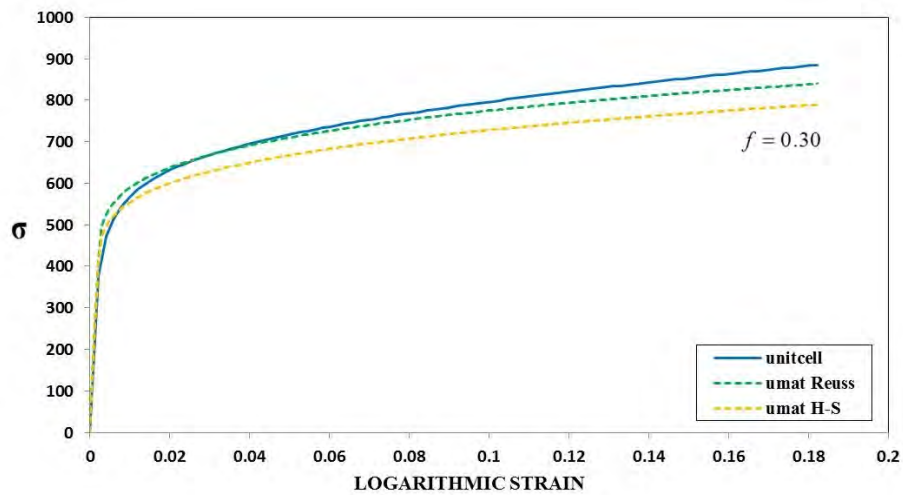Figure 4.9: Comparison of stress-strain curves for f =20%.

- **Model III (f=30%)**

Figure 4.10: Comparison of stress-strain curves for f =30%.

- **Model IV (f=40%)**
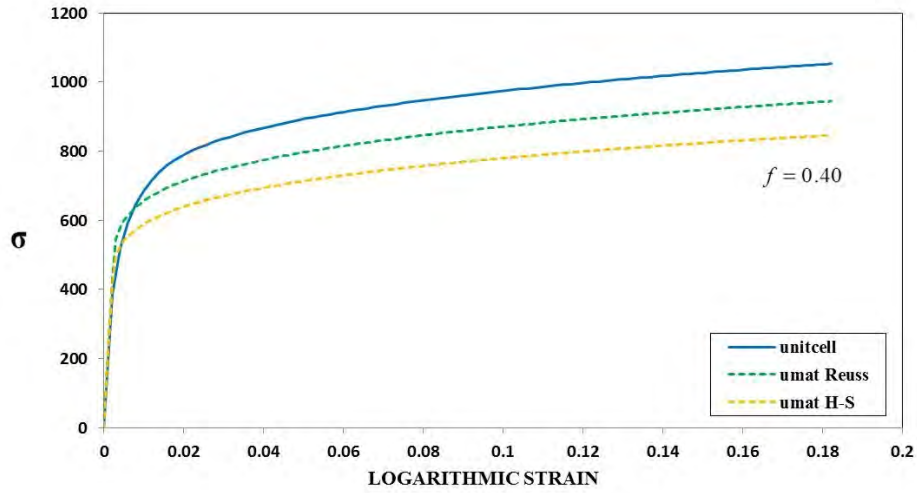

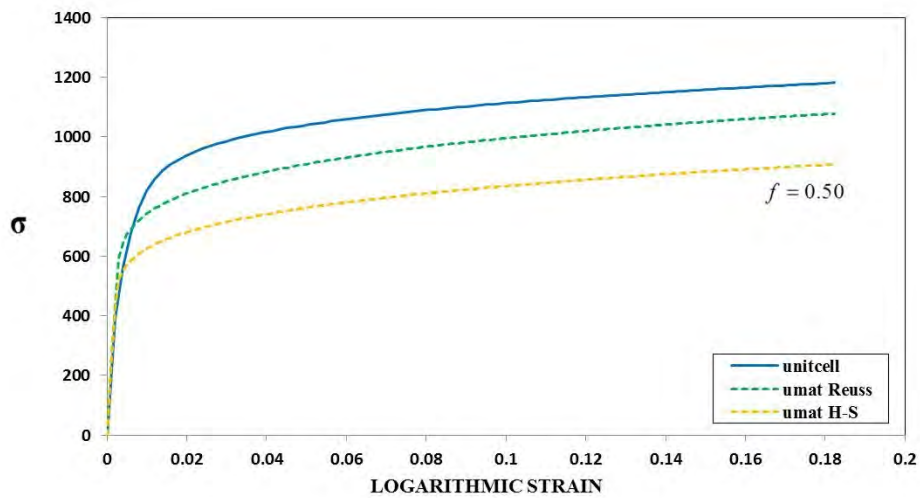Figure 4.11: Comparison of stress-strain curves for f =40%.

- **Model V (f=50%)**

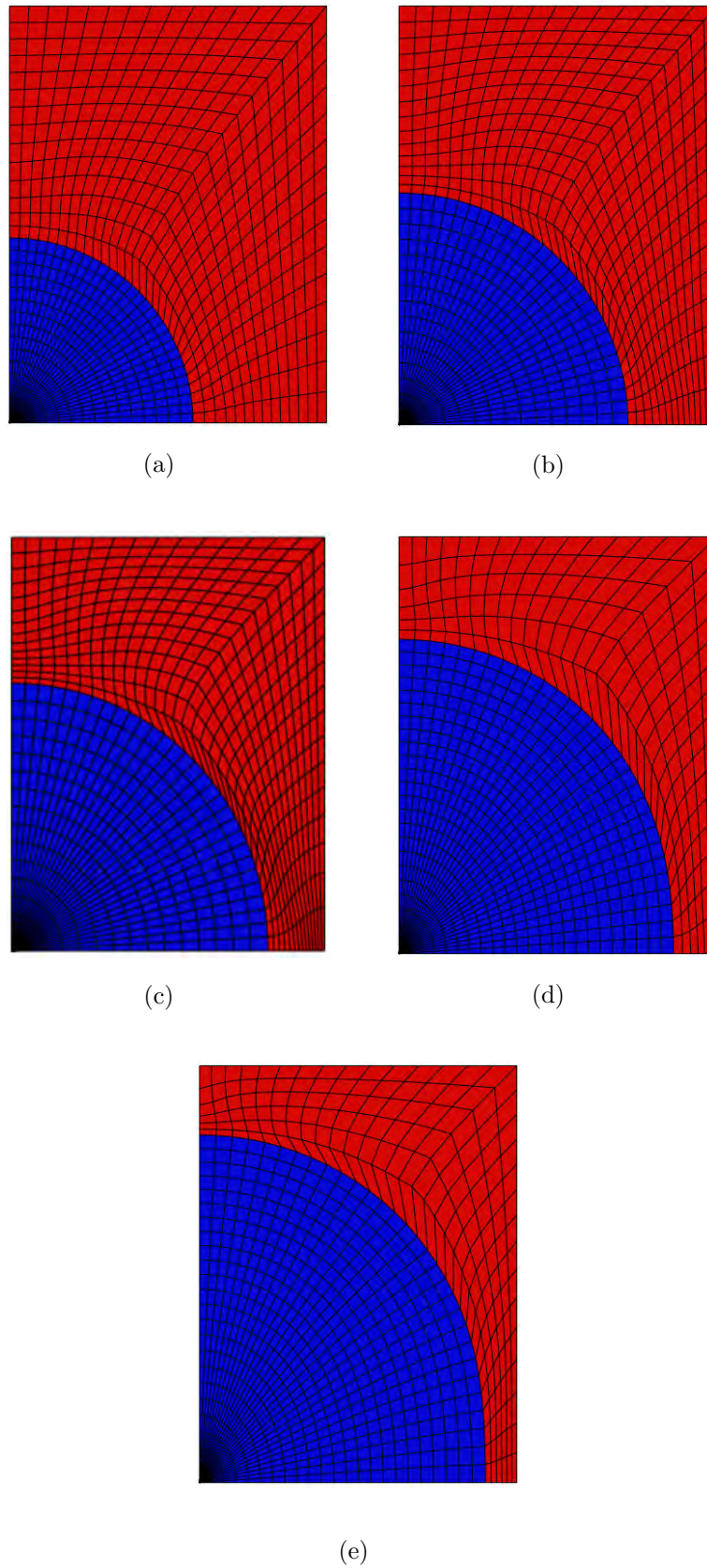Figure 4.12: Comparison of stress-strain curves for f =50%.

Figure 4.13: Deformed finite element meshes at the final elongation for (a) f =10%, (b) f =20%, (c) f =30%, (d) f =40% and (e) f =50%. The blue elements correspond to the martensitic particles and the red elements are the austenitic matrix.
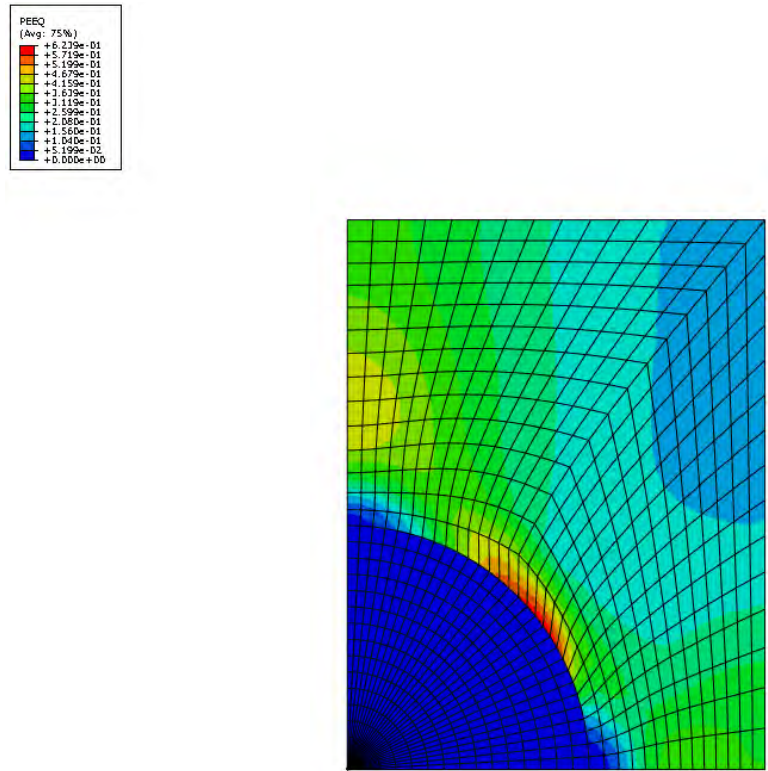
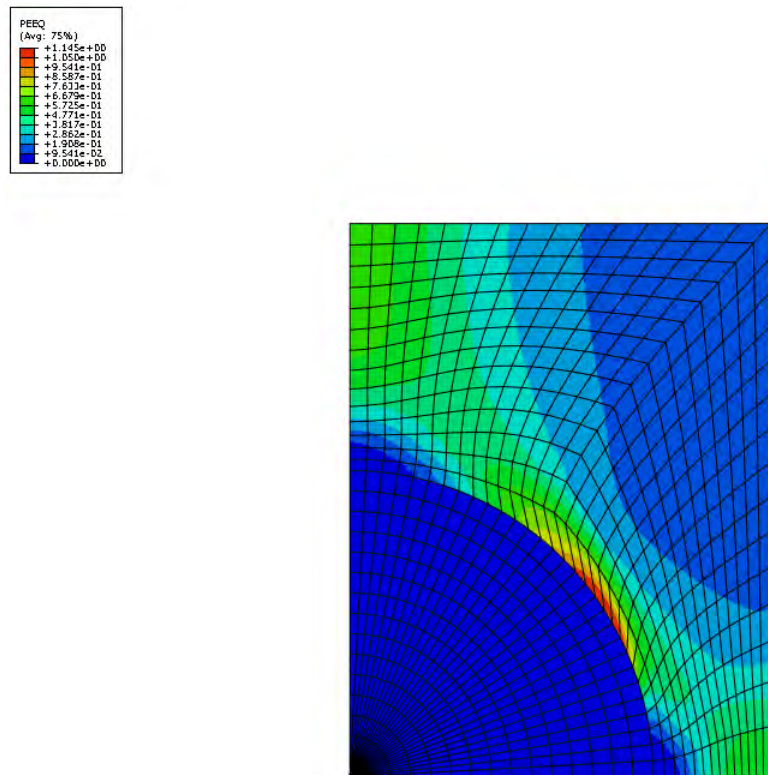Figure 4.14: Contours of equivalent plastic strain for f =10%.

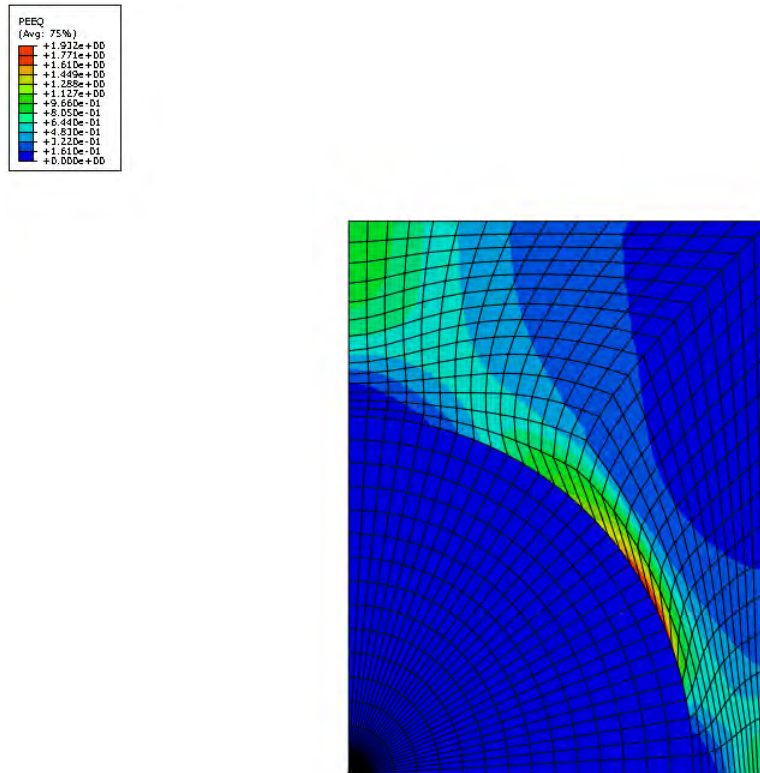Figure 4.15: Contours of equivalent plastic strain for f =20%.

Figure 4.16: Contours of equivalent plastic strain for f =30%.
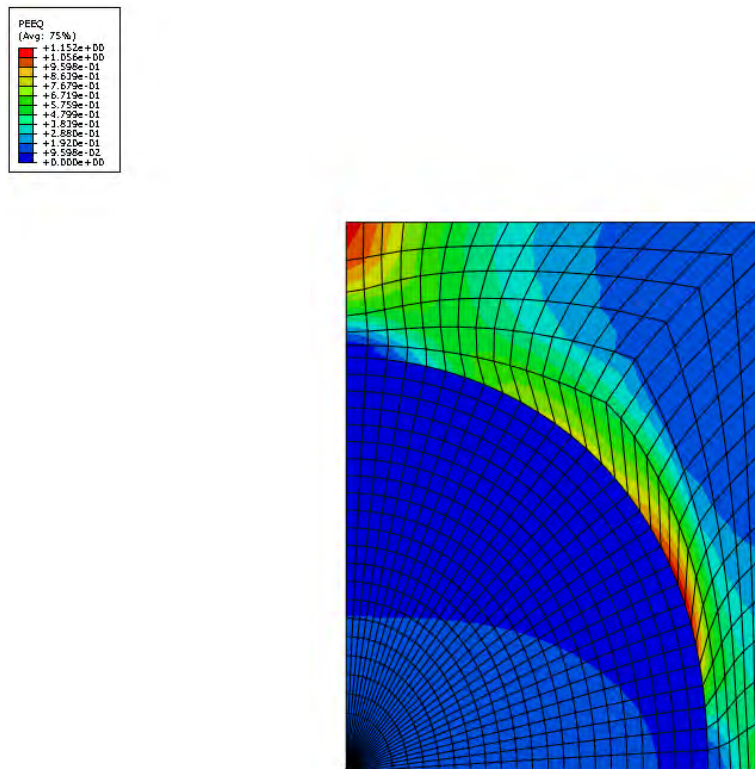

Figure 4.17: Contours of equivalent plastic strain for f =40%.

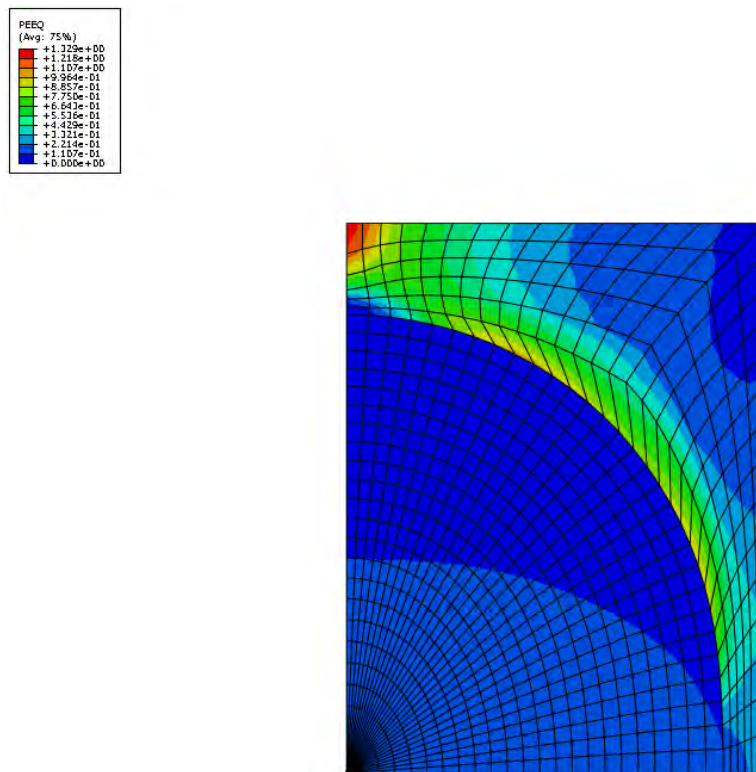Figure 4.18: Contours of equivalent plastic strain for f =50%.

Chapter 5

3-D finite-element simulations

5.1 Introduction

In order to compare the above theoretical results of homogenization theory and unit cell calculations with a separate solution, in this chapter we work out full 3D finite-element(FE) simulations of the large-deformation response of a two-phase elastoplastic material. To simulate the randomness and isotropy of the microstructure, we consider infinite periodic media made up of the repetition of cubic unit cells with sides of length $L = 1$ and unit volume ($L^3 = 1$) containing a random distribution of a large number of spherical particles. In this thesis we examine only distributions with particles of the same size (monodisperse).

5.2 Monodisperse microstructures

The monodisperse microstructure is a periodic cubic unit cell of volume $L^3 = 1$ containing a random dispersion of 30 non-overlapping identical spheres. Evidently, the accuracy of the solution and the computer time to solve the problem increases with the number of particles in the unit cell, and this figure was dictated by a compromise between the two factors. The final particle arrangement has to be statistically isotropic (all directions in the unit cell are equivalent) and, in addition, it should be suitable for finite element discretization. Both conditions can be fulfilled using the Random Sequential Adsortion (RSA) algorithm to generate the coordinates of the particle centers (Rintoul and Torquato, 1997).
According to this method, the particle center positions are generated randomly and sequentially. The sequential addition of particles is constrained so that the distance between the particles with other particles and with the boundaries of the cubic unit cell take a minimum value that guaranties adequate spatial discretization(see, e.g., Segurado and Llorca, 2002; Fritzen *et al.*, 2012), namely:

- The center-to-center distance between a new particle i in the sequential algorithm and any previously accepted particle $j = 1, 2, ..., i - 1$ has to exceed the minimum value $s_1 = 2 R_m(1 + d_1)$, where the offset distance d_1 is fixed here at $d_1 = 0.02$. This condition can be compactly written in the form

$$\left\| \mathbf{X}^i - \mathbf{X}^j - \mathbf{h} \right\| \geq s_1. \tag{5.1}$$

where $\mathbf{X}^i$ ($\mathbf{X}^j$) denotes the location of the center of particle i (j) and $\mathbf{h}$ is a vector with entries 0, L or $-L$ for each of its three Cartesian components with respect to the principal axes of the cubic unit cell.

- The particles should be sufficiently distant from the boundaries of the unit cell as enforced by the inequalities

$$\left\| X_k^i - R_m \right\| \geq s_2 \qquad \text{and} \qquad \left\| X_k^i + R_m - L \right\| \geq s_2 \qquad (k = 1, 2, 3), \tag{5.2}$$

where $s_2 = d_2 \, R_m$ with d_2 being fixed here at $d_2 = 0.05$.

In the above expressions

$$R_m = L \left(\frac{3 \, c}{4 \, \pi \, N} \right)^{1/3} \tag{5.3}$$

stands for the radius of the particles, where N is the number of particles in the unitcell. Figure 5.1 shows typical distributions of particles for $f = 0.1$ and 0.2.

The RSA algorithm, in combination with Equations (5.1) and (5.2), was used to generate the particle center coordinates up to a sphere volume fraction $f = 0.2$. Above this volume fraction, it was not possible to accommodate 30 particles in the unit cell fulfilling all the conditions imposed by Equations (5.1) and (5.2). Unit cells with f above the "jamming limit" (the final state of the process whereby no particles can be added) can be generated using particles with different sizes (polydisperse).
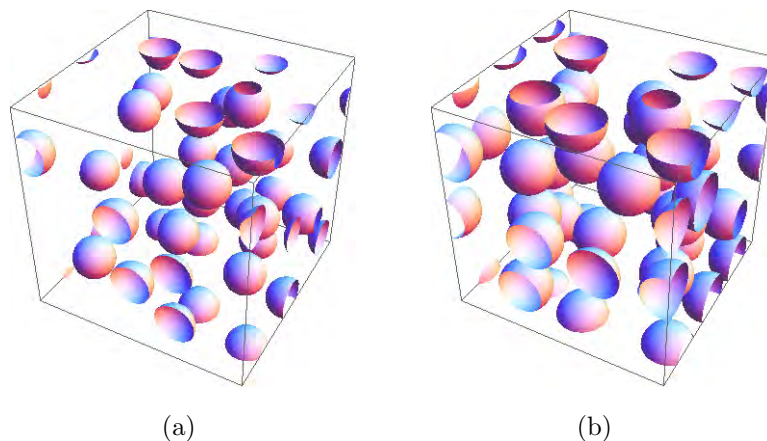

(a)   (b)

Figure 5.1: Representative unit cells of unit volume $L^3 = 1$ containing $N = 30$ randomly distributed spherical particles of monodisperse sizes with two different concentrations: (a) $f = 0.1$ and (b) $f = 0.2$.

5.3 Meshing and computation of the overall nonlinear response

Finite element discretizations of a cubic unit cell were created from the particle center distributions using the mesh generator code NETGEN (Schöberl, 1997), which has the capability to create periodic meshes as required here. Ten-node tetrahedral hybrid elements are utilized in order to handle exactly (in a numerical sense) the incompressible behavior of the elastoplastic matrix and of the rigid particles. The "hybrid" elements C3D10H in ABAQUS were used in the calculations (see ABAQUS, Documentation, Version 6.11, 2011). Figure 5.2 shows three finite element meshes of increasing refinement for a distribution of monodisperse particles with concentration $f = 0.2$.
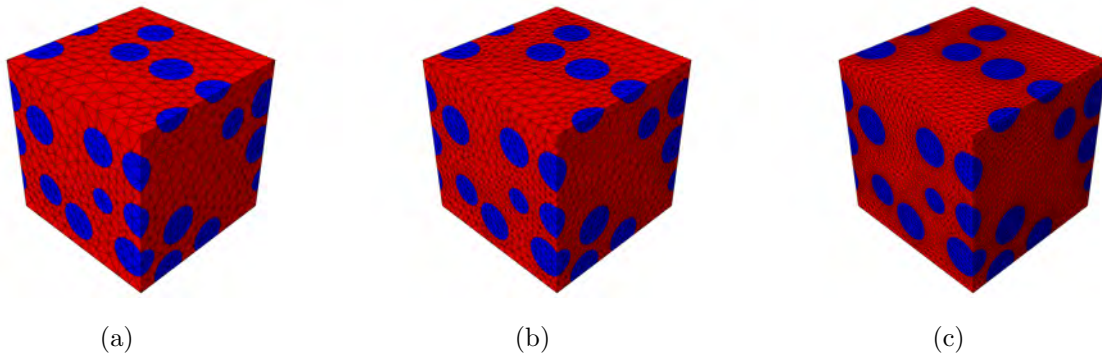

| (a) | (b) | (c) |

Figure 5.2: Three representative meshes in the undeformed configuration for a distribution of monodisperse particles with concentration $f = 0.2$: (a) moderate mesh, (b) fine mesh, and (c) very fine mesh

Periodic boundary conditions were applied to the unit cell faces. The boundary conditions on the cube faces can be expressed as

$$
\begin{aligned}
u_k \left(L, X_2, X_3 \right) - u_k \left(0, X_2, X_3 \right) &= \left(F_{k1} - \delta_{k1} \right) L, \\
u_k \left(X_1, L, X_3 \right) - u_k \left(X_1, 0, X_3 \right) &= \left(F_{k2} - \delta_{k2} \right) L, \\
u_k \left(X_1, X_2, L \right) - u_k \left(X_1, X_2, 0 \right) &= \left(F_{k3} - \delta_{k3} \right) L,
\end{aligned}
\tag{5.4}
$$

where the components u_k and X_k $(k = 1, 2, 3)$ refer to a Cartesian frame of reference with origin placed at a corner of the cubic unit cell whose axes are aligned with the principal axes of the cubic unit cell, δ_{kl} denotes the Kronecker delta, and **F** is the prescribed average deformation gradient. As a practical remark, we note that the periodic boundary conditions (5.4) can be expediently implemented in ABAQUS by using the "*EQUATION" option to couple the nodes of opposite sides of the cubic unit cells.

In the comparisons with the predictions of the homogenization theory and unit cell calculations that follow, all finite element results are computed by following an incremental loading path, at each step of which the incremental equilibrium equations are solved directly

in ABAQUS. We utilize the default dual convergence criterion in this code (see ABAQUS, Documentation, Version 6.11, 2011), namely, the permissible ratio of the largest solution correction to the largest corresponding incremental solution is set at $|\Delta\mathbf{u}|\,/\,|\mathbf{u}_{\max}| = 10^{-2}$ and the permissible ratio of the largest residual to the corresponding average force norm is set at $R_{tol} = 5 \times 10^{-3}$. Whenever one of these criteria is not satisfied the computations are stopped. This typically happens whenever the elements in between two particles become exceedingly distorted because of the locally large deformations involved.

5.4 Comparison of the predictions of the homogenization theory and the unit cell calculations with 3-D finite-element simulations

The predictions of the homogenization theory and the unit cell problem have been calculated as described in section 4.6. Regarding the 3-D finite-element simulations, for volume fractions $f = 0.1$ and $f = 0.2$ we used monodisperse microstructures, while for $f = 0.3$, $f = 0.4$ and $f = 0.5$ we used polydisperse microstructures, since monodisperse microstructures couldn't be generated.

The results of the four methods are compared in Figures 5.3-5.12. It is found that the predictions of the four methods agree reasonably well in the first two cases with $f = 0.1$ and $f = 0.2$. But, as the volume fraction of the martensite increases we observe that the predictions differ, with the Reuss model agreeing with the 3-D finite-element simulations. At this point the differences between the predictions of the unit cell calculations and the 3-D finite-element simulations should be emphasized, noting that the most accurate are those of the 3-D finite-element simulations. The deformed finite element meshes at the final elongation of 20% are shown in Figure 5.13.
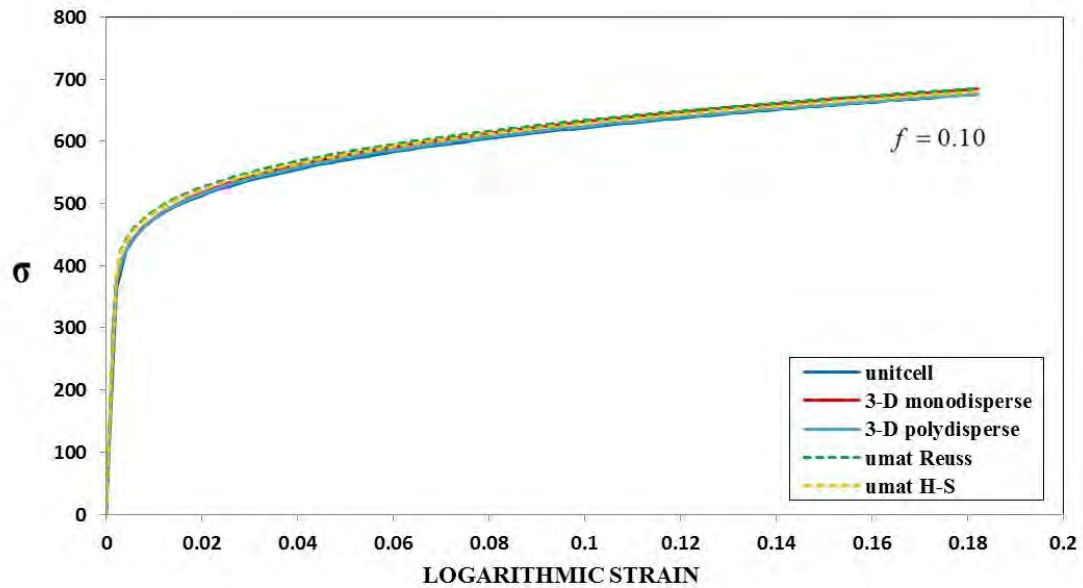
• **Model I (f=10%)**

Figure 5.3: Comparison of stress-strain curves for f =10%.
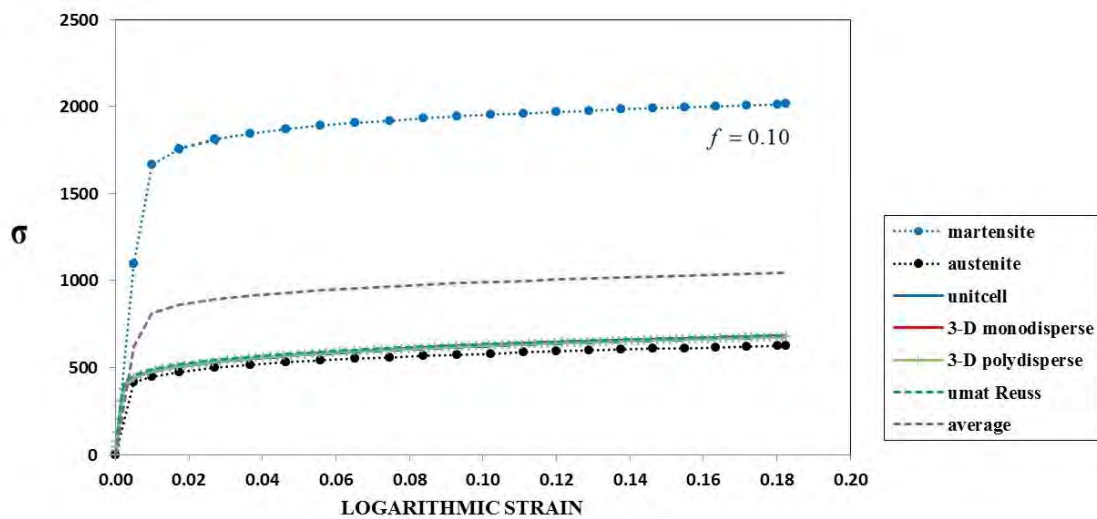

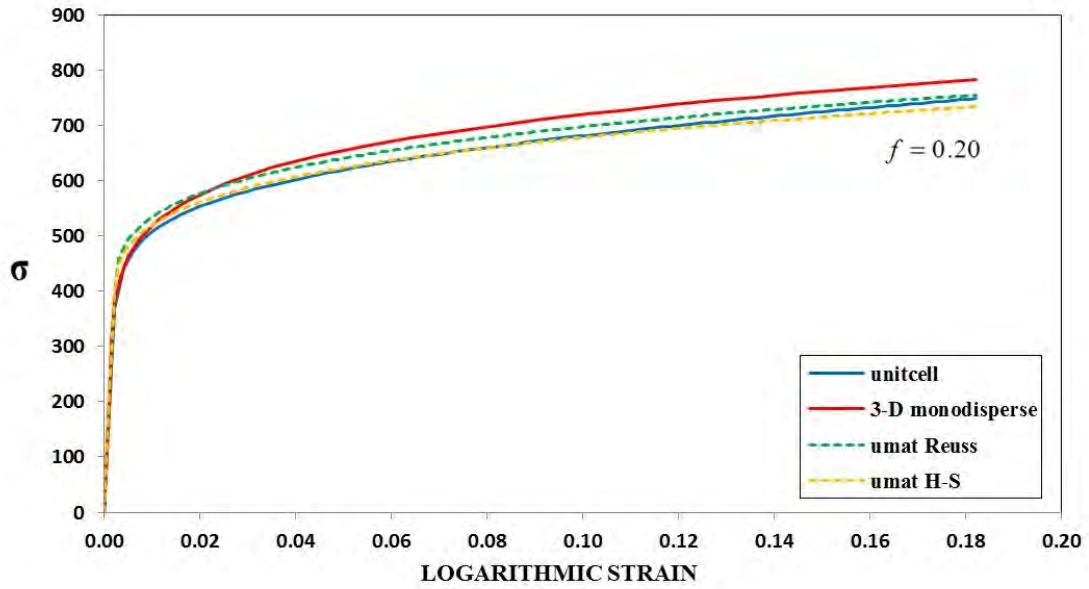Figure 5.4: Comparison of stress-strain curves for f =10%.

- **Model II (f=20%)**

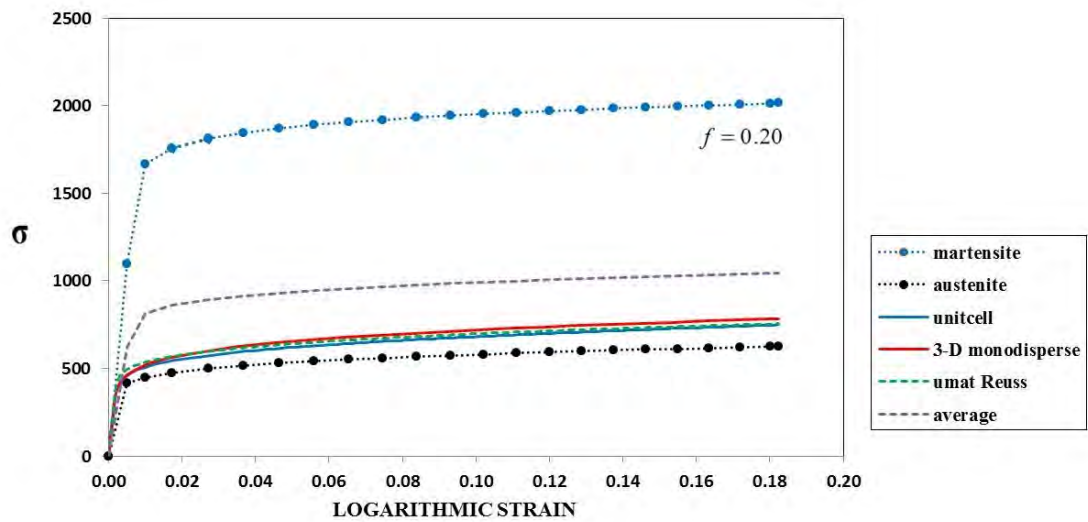Figure 5.5: Comparison of stress-strain curves for f =20%.

Figure 5.6: Comparison of stress-strain curves for f =20%.

- **Model III (f=30%)**

Figure 5.7: Comparison of stress-strain curves for f =30%.

Figure 5.8: Comparison of stress-strain curves for f =30%.
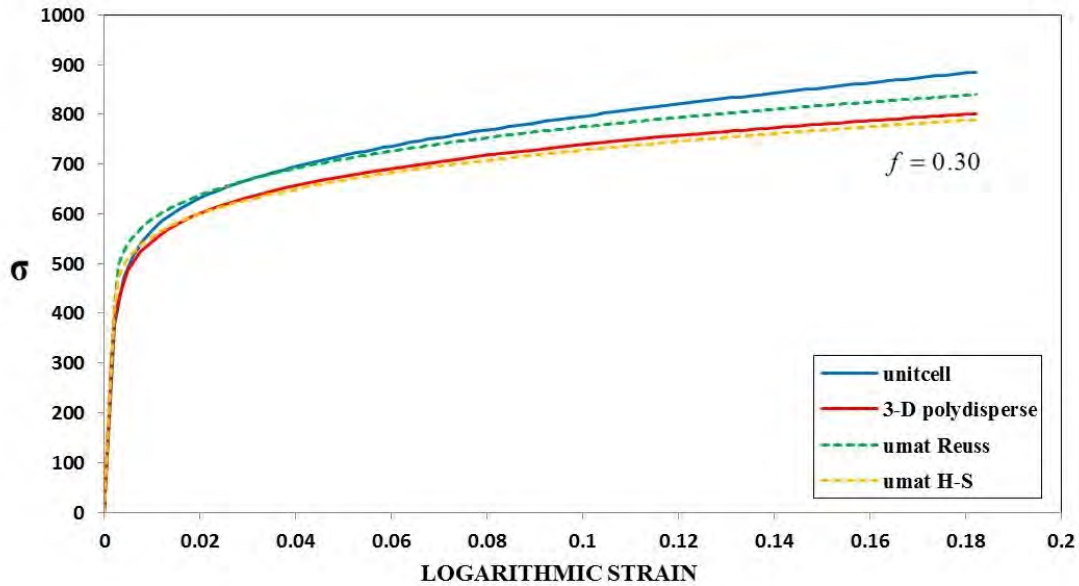
- **Model IV (f=40%)**

Figure 5.9: Comparison of stress-strain curves for f =40%.

Figure 5.10: Comparison of stress-strain curves for f =40%.

- **Model V (f=50%)**

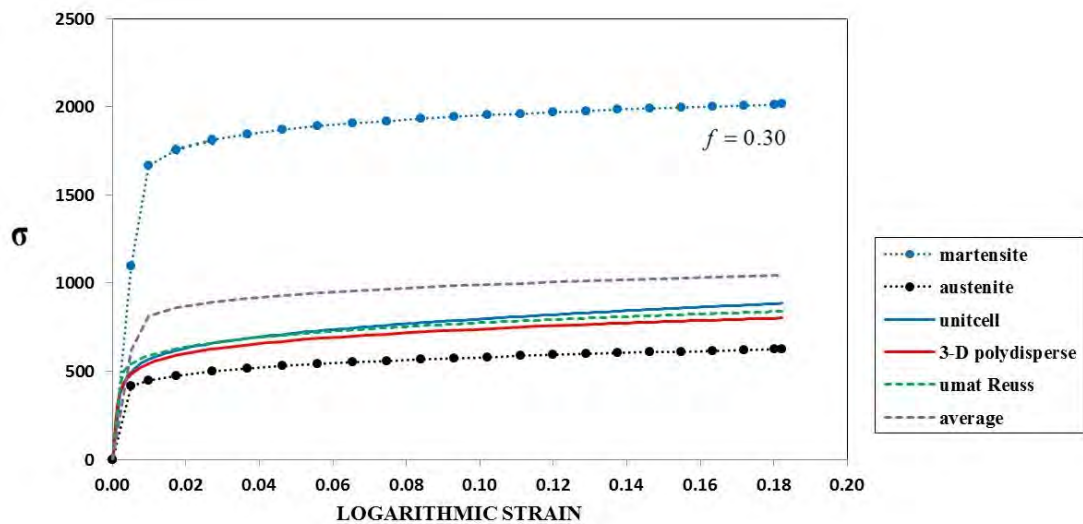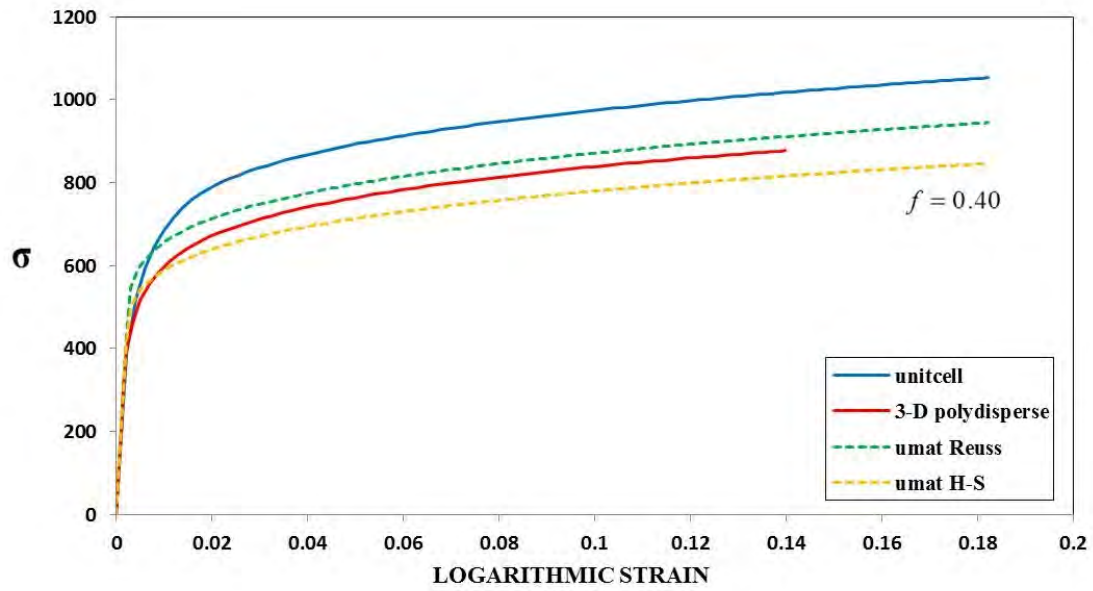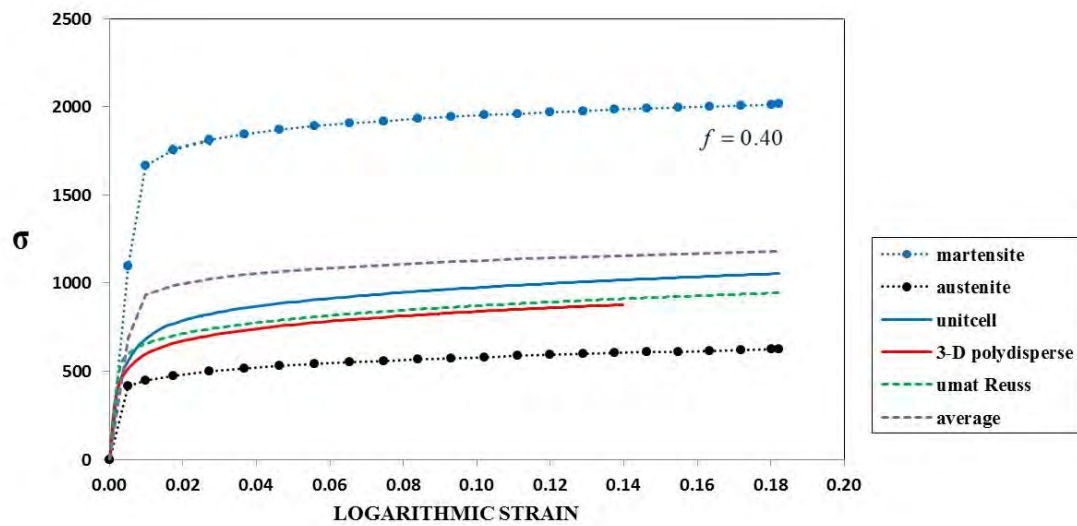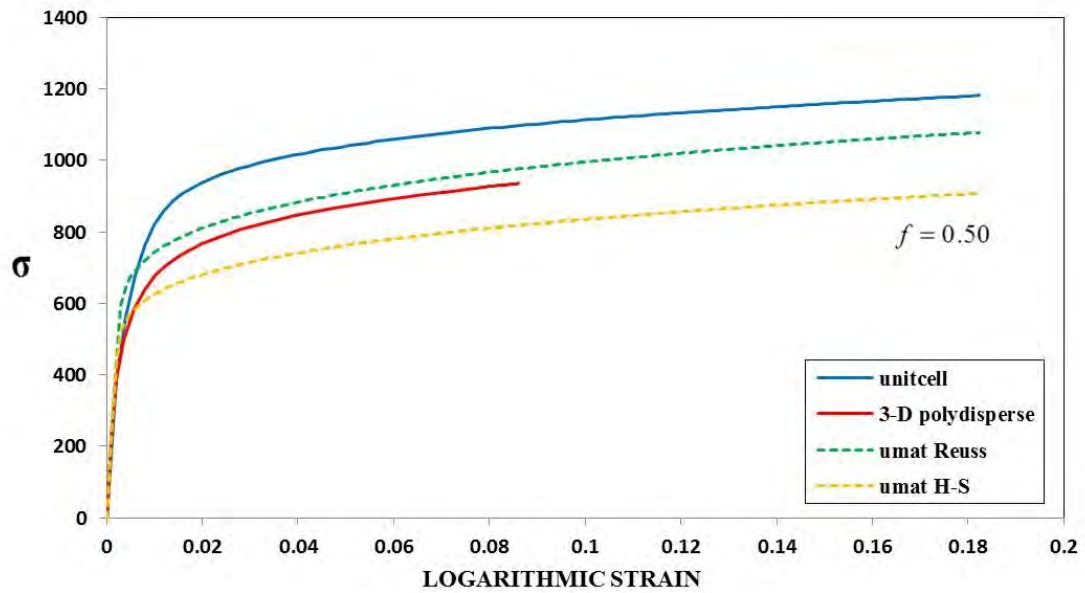

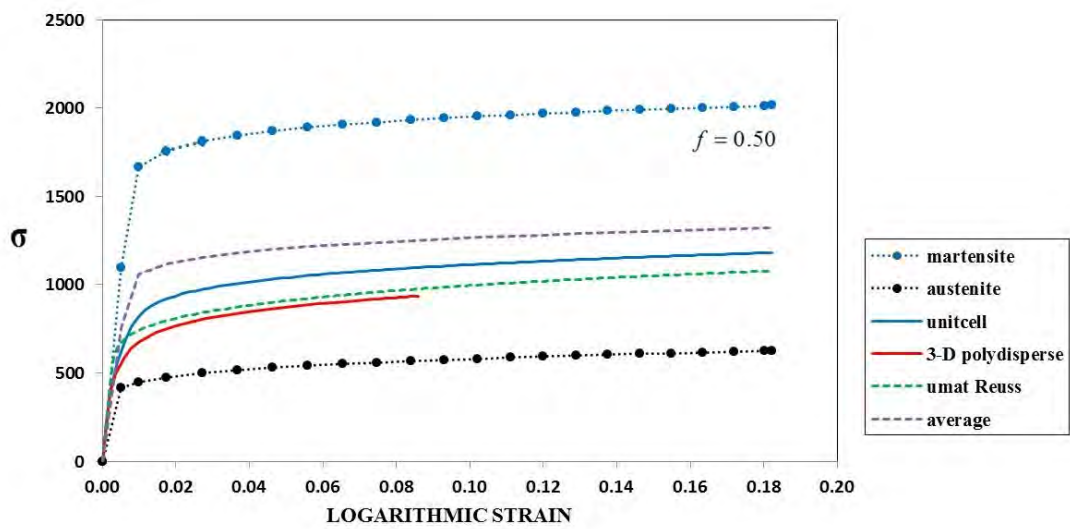Figure 5.11: Comparison of stress-strain curves for f =50%.

Figure 5.12: Comparison of stress-strain curves for f =50%.
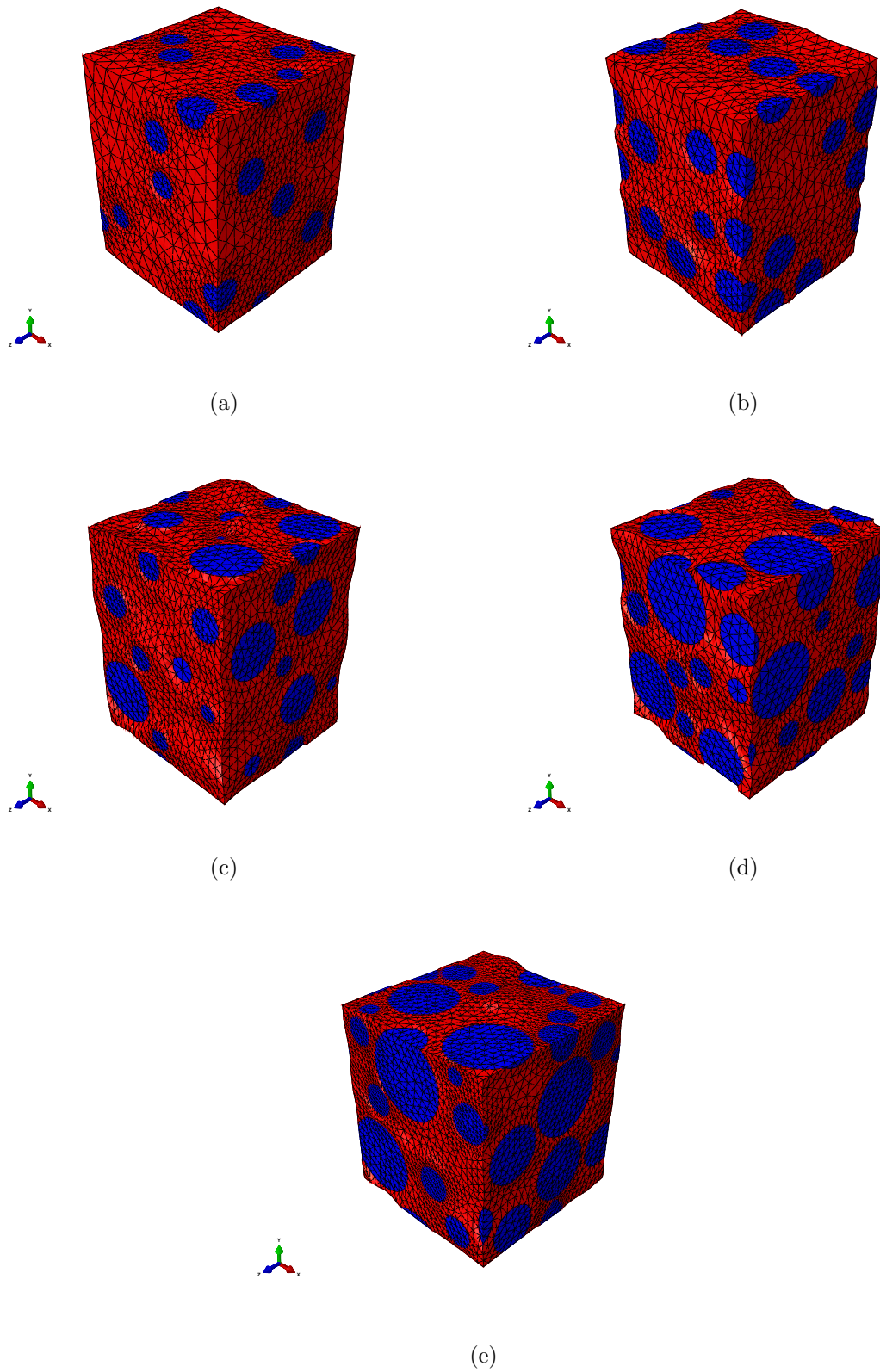
Figure 5.13: Deformed finite element meshes at the final elongation for (a) f =10%, (b) f =20%, (c) f =30%, (d) f =40%, and (e) f =50%. The blue elements correspond to the martensitic particles and the red elements are the austenitic matrix.

Bibliography

[1] ABAQUS, Analysis User's Manual, Version 6.11, © Dassault Systémes, 2011.

[2] N. Aravas and P. Ponte Castañeda, 'Numerical methods for porous metals with deformation-induced anisotropy', *Comput. Methods Appl. Mech. Engrg* **193** (2004) 3767–3805.

[3] F. Fritzen, S. Forest, T. Böhlke, D. Kondo, and T. Kanit, 'Computational homogenization of elasto-plastic porous metals', *Int. J. Plasticity* **29** (2012) 102–119.

[4] Z. Hashin and S. Shtrikman, 'A variational approach to the theory of elastic behavior of multiphase materials', *J. Mech. Phys. Solids* **11** (1963) 127–140.

[5] R. Hill, 'A self consistent mechanics of composite materials', *J. Mech. Phys. Solids* **13** (1965) 213–222.

[6] T.J.R. Hughes, The finite element method, Dover Publications, (2000).

[7] M. Kailasam and P. Ponte Castañeda, 'A general constitutive theory for linear and nonlinear particulate media with microstructure evolution', *J. Mech. Phys. Solids* **46** (1998) 427–465.

[8] O. Lopez-Pamies, T. Goudarzi, and K. Danas, 'The nonlinear elastic response of suspensions of rigid inclusions in rubber: II — A simple explicit approximation for finite-concentration suspension', *J. Mech. Phys. Solids* **61** (2013) 19–37.

[9] I. Papatriantafillou, 'TRIP steels: Constitutive modeling and computational issues', *Ph.D. Thesis, University of Thessaly* (2005).

[10] I. Papatriantafillou, M. Agoras, N. Aravas, and G. Haidemenopoulos, 'Constitutive modeling and finite element methods for TRIP steels', *Comput. Methods Appl. Mech. Engrg.* **195** (2006) 5094–5114.

[11] T. Naturani, G.B. Olson and M. Cohen, 'Constitutive flow relations for austenitic steels during strain-induced martensitic transformation', *J. Mech. Phys. Solids* **43** (1982) 247–257.

[12] Technical Steel Research: 'Modeling of mechanical properties and local deformation of high-strength multi-phase steels', Final Report, European Commission,Contract No. 7210-Pr/044, 2002.

[13] P. Ponte Castañeda, 'The effective mechanical properties of nonlinear isotropic solids', *J. Mech. Phys. Solids* **39** (1991) 45–71.

[14] P. Ponte Castañeda, 'New variational principles in plasticity and their application to composite materials', *J. Mech. Phys. Solids* **40** (1992) 1757–1788.

[15] P. Ponte Castañeda, 'Nonlinear composite materials: effective constitutive behavior and microstructure evolution', *Continuum Micromechanics,* CISM Courses and Lectures, ed. P. Suquet, vol. 377 (1997) 131–195. Springer-Verlag.

[16] P. Ponte Castañeda and G. deBotton, 'On the homogenized yield strength of two-phase composites', *Proc. Roy. Soc. London A* **438** (1992) 419–431.

[17] M.D. Rintoul and S. Torquato, 'Reconstruction of the structure of dispersions', *J. Colloid Interface Sci.* **186** (1997) 467–476.

[18] J. Schöberl, 'Netgen an advancing front 2d/3d-mesh generator based on abstract rules', *Comput. Visual. Sci.* **1** (1997) 41–52.

[19] J. Segurado and J. Llorca, 'A numerical approximation to the elastic properties of sphere-reinforced composites', *J. Mech. Phys. Solids* **50** (2002) 2107–2121.

[20] P. Suquet, 'Overall properties of nonlinear composites: A modified secant moduli theory and its link with Ponte Castañeda's nonlinear variational procedure', *C. R. Acad. Sci. Paris, II b* **320** (1995) 563–571.

[21] D.R.S. Talbot and J.R. Willis, 'Variational principles for inhomogeneous nonlinear media', *IMA J. Appl. Math.* **35** (1985) 39–54.

Appendix A

The usual stationarity conditions of (2.31) (valid for $y^{(r)} > 0$, i.e., $y^{(r)} \neq 0$) are

$$\frac{\partial}{\partial y^{(i)}} \left(\frac{\sigma_\infty^2}{F} \right) = 0 \quad \Rightarrow \quad \frac{\partial \sigma_\infty^2}{\partial y^{(i)}} \frac{1}{F} - \frac{\sigma_\infty^2}{F^2} \frac{\partial F}{\partial y^{(i)}} = 0 \quad \Rightarrow \quad \left(\frac{\partial \sigma_\infty^2}{\partial y^{(i)}} - \frac{\sigma_\infty^2}{F} \frac{\partial F}{\partial y^{(i)}} \right) \frac{1}{F} = 0 \quad \text{(A.1)}$$

$$\frac{\partial F}{\partial y^{(i)}} \underbrace{\frac{\sigma_\infty^2}{F}}_{\bar{\sigma}_0^2} - \frac{\partial \sigma_\infty^2}{\partial y^{(i)}} = 0 \quad \text{or} \quad \frac{\partial F}{\partial y^{(i)}} \bar{\sigma}_0^2 - \frac{\partial \sigma_\infty^2}{\partial y^{(i)}} = 0 \qquad i = 2, 3, \ldots, N. \quad \text{(A.2)}$$

We have that

$$F = \frac{T_1}{T_2}, \qquad \frac{\partial F}{\partial y^{(i)}} = \left(\frac{1}{T_1} \frac{\partial T_1}{\partial y^{(i)}} - \frac{1}{T_2} \frac{\partial T_2}{\partial y^{(i)}} \right) F, \qquad i = 1, 2, \ldots, N, \quad \text{(A.3)}$$

$$\sigma_\infty^2 = \sum_{r=1}^{N} c^{(r)} \left(\sigma_0^{(r)} \right)^2 y^{(r)}, \qquad \frac{\partial \sigma_\infty^2}{\partial c^{(i)}} = \left(\sigma_0^{(i)} \right)^2 y^{(i)}, \qquad \frac{\partial \sigma_\infty^2}{\partial \sigma_0^{(i)}} = 2 \, c^{(i)} \, \sigma_0^{(i)} \, y^{(i)}, \quad \text{(A.4)}$$

$$\frac{\partial \sigma_\infty^2}{\partial y^{(i)}} = c^{(i)} \left(\sigma_0^{(i)} \right)^2, \qquad i = 1, 2, \ldots, N. \quad \text{(A.5)}$$

The stationarity conditions (A.2) can be written in the form

$$\left(\frac{\partial T_1}{pr y^{(i)}} \frac{1}{T_2} - \frac{T_1}{T_2^2} \frac{\partial T_2}{\partial y^{(i)}} \right) \frac{\sigma_\infty^2}{T_1 / T_2} - c^{(i)} \left(\sigma_0^{(i)} \right)^2 = 0 \quad \Rightarrow \quad \text{(A.6)}$$

$$A^{(i)} \left(y^{(s)} \right) \equiv \left(\frac{1}{T_1} \frac{\partial T_1}{\partial y^{(i)}} - \frac{1}{T_2} \frac{\partial T_2}{\partial y^{(i)}} \right) \sigma_\infty^2 - c^{(i)} \left(\sigma_0^{(i)} \right)^2 = 0, \quad i = 2, 3, \ldots, N, \quad y^{(r)} \neq 0. \quad \text{(A.7)}$$

The solution of the constrained optimization problem is found by using some standard package and equations (A.7) are valid provided that $y^{(r)} \neq 0$ (in fact > 0). Let the optimal values be $\left(y^{(2)}, y^{(3)}, \ldots, y^{(N)} \right) = \left(\hat{y}^{(2)}, \hat{y}^{(3)}, \ldots, \hat{y}^{(N)} \right) \geq 0$, where $\hat{y}^{(r)} = \hat{y}^{(r)} \left(c^{(s)}, \sigma_0^{(s)} \right)$.

Variation of $\bar{\sigma}_0$ w.r.t. $c^{(i)}$ and $\sigma_0^{(i)}$

$$\bar{\sigma}_0^2 = \frac{\sigma_\infty^2 \left(\hat{y}^{(s)}, c^{(s)}, \sigma_0^{(s)} \right)}{F \left(\hat{y}^{(s)}, c^{(s)} \right)} \qquad \Rightarrow$$

$$2\,\bar{\sigma}_0 \frac{\partial \bar{\sigma}_0}{\partial c^{(i)}} = \left(\frac{\partial \sigma_\infty^2}{\partial c^{(i)}} + \sum_{j=2}^{N} \frac{\partial \sigma_\infty^2}{\partial \hat{y}^{(j)}} \frac{\partial \hat{y}^{(j)}}{\partial c^{(i)}} \right) \frac{1}{F} - \underbrace{\frac{\sigma_\infty^2}{F^2}}_{\bar{\sigma}_0^2/F} \left(\frac{\partial F}{\partial c^{(i)}} + \sum_{j=2}^{N} \frac{\partial F}{\partial \hat{y}^{(j)}} \frac{\partial \hat{y}^{(j)}}{\partial c^{(i)}} \right) =$$

$$= \frac{1}{F} \left[\frac{\partial \sigma_\infty^2}{\partial c^{(i)}} - \bar{\sigma}_0^2 \frac{\partial F}{\partial c^{(i)}} + \sum_{j=2}^{N} \left(\frac{\partial \sigma_\infty^2}{\partial \hat{y}^{(j)}} \frac{\partial \hat{y}^{(j)}}{\partial c^{(i)}} - bar\sigma_0^2 \frac{\partial F}{\partial \hat{y}^{(j)}} \frac{\partial \hat{y}^{(j)}}{\partial c^{(i)}} \right) \right] =$$

$$= \frac{1}{F} \left[\frac{\partial \sigma_\infty^2}{\partial c^{(i)}} - \bar{\sigma}_0^2 \frac{\partial F}{\partial c^{(i)}} + \sum_{j=2}^{N} \underbrace{\left(\frac{\partial \sigma_\infty^2}{\partial \hat{y}^{(j)}} - \bar{\sigma}_0^2 \frac{\partial F}{\partial \hat{y}^{(j)}} \right)}_{0,\ \text{see}(A.2)} \frac{\partial \hat{y}^{(j)}}{\partial c^{(i)}} \right] \quad \Rightarrow \qquad (A.8)$$

$$\frac{\partial \bar{\sigma}_0}{\partial c^{(i)}} = \frac{1}{2\,\bar{\sigma}_0\,F} \left(\frac{\partial \sigma_\infty^2}{\partial c^{(i)}} - \bar{\sigma}_0^2 \frac{\partial F}{\partial c^{(i)}} \right), \qquad i = 1, 2, 3, \ldots, N, \qquad (A.9)$$

where we took into account the optimality condition (A.2), namely $\frac{\partial \sigma_\infty^2}{\partial \hat{y}^{(j)}} - \bar{\sigma}_0^2 \frac{\partial F}{\partial \hat{y}^{(j)}} = 0$.

Note
1) If a $y^{(j)} = 0$, so that (A.2) and (A.7) are not valid, the quantity $\frac{\partial \sigma_\infty^2}{\partial \hat{y}^{(j)}} - \bar{\sigma}_0^2 \frac{\partial F}{\partial \hat{y}^{(j)}}$ still vanishes because $\frac{\partial \sigma_\infty^2}{\partial \hat{y}^{(j)}} = \frac{\partial F}{\partial \hat{y}^{(j)}} = 0$, i.e., equations (A.9) are valid even for those i that correspond to $y^{(i)} = 0$.

2) All volume fractions $c^{(i)}$ are treated as independent variables. The constraint $\sum_{i=1}^{N} c^{(i)} = 1$ is taken care by the evolution equations of the volume fractions.
The quantities $\partial \sigma_\infty^2 / \partial c^{(i)}$ are defined by (A.5). Similarly

$$\frac{\partial \bar{\sigma}_0}{\partial \sigma_0^{(i)}} = \frac{1}{2\,\bar{\sigma}_0\,F} \frac{\partial \sigma_\infty^2}{\partial \sigma_0^{(i)}} \qquad i = 1, 2, \ldots, N, \qquad (A.10)$$

where the quantities $\partial \sigma_\infty^2 / \partial \sigma_0^{(i)}$ are defined by (A.5).

Variation of $\hat{y}^{(i)}$ with respect to $c^{(i)}$ and $\sigma_0^{(i)}$
The derivatives $\frac{\partial \hat{y}^{(i)}}{\partial \sigma_0^{(j)}}$ are needed for the calculation of $\frac{\partial \alpha^{(i)}}{\partial \sigma_0^{(j)}} = \sum_{k=1}^{N} \frac{\partial \alpha^{(i)}}{\partial y^{(k)}} \frac{\partial y^{(k)}}{\partial \sigma_0^{(j)}}$ in equation (B.6) below. The stationarity conditions that define $\hat{y}^{(r)} = \hat{y}^{(r)} \left(c^{(s)}, \sigma_0^{(s)} \right)$ are given by equations (A.7):

$$A^{(i)} \equiv \left[\frac{1}{T_1\left(\hat{y}^{(r)}, c^{(r)}\right)} \frac{\partial T_1}{\partial y^{(i)}} \left(\hat{y}^{(r)}, c^{(r)}\right) - \frac{1}{T_2\left(\hat{y}^{(r)}, c^{(r)}\right)} \frac{\partial T_2}{\partial y^{(i)}} \left(\hat{y}^{(r)}, c^{(r)}\right) \right] \sigma_\infty^2 \left(\hat{y}^{(r)}, c^{(r)}, \sigma_0^{(r)}\right) -$$

$$- c^{(i)} \left(\sigma_0^{(i)} \right)^2 = 0, \qquad i = 2, 3, \ldots, N, \qquad \hat{y}^{(i)} \neq 0. \quad (A.11)$$

In that case

$$
\frac{\partial A^{(i)}}{\partial c^{(r)}} = \left[-\frac{1}{T_1^2} \left(\frac{\partial T_1}{\partial c^{(r)}} + \sum_{j=2}^{N} \frac{\partial T_1}{\partial \hat{y}^{(j)}} \frac{\partial \hat{y}^{(j)}}{\partial c^{(r)}} \right) \frac{\partial T_1}{\partial \hat{y}^{(i)}} + \frac{1}{T_1} \left(\frac{\partial^2 T_1}{\partial \hat{y}^{(i)} \partial c^{(r)}} + \sum_{j=2}^{N} \frac{\partial^2 T_1}{\partial \hat{y}^{(i)} \partial \hat{y}^{(j)}} \frac{\partial \hat{y}^{(j)}}{\partial c^{(r)}} \right) + \right.
$$

$$
+ \frac{1}{T_2^2} \left(\frac{\partial T_2}{\partial c^{(r)}} + \sum_{j=2}^{N} \frac{\partial T_2}{\partial \hat{y}^{(j)}} \frac{\partial \hat{y}^{(j)}}{\partial c^{(r)}} \right) \frac{\partial T_2}{\partial \hat{y}^{(i)}} - \left. \frac{1}{T_2} \left(\frac{\partial^2 T_2}{\partial \hat{y}^{(i)} \partial c^{(r)}} + \sum_{j=2}^{N} \frac{\partial^2 T_2}{\partial \hat{y}^{(j)} \partial \hat{y}^{(i)}} \frac{\partial \hat{y}^{(j)}}{\partial c^{(r)}} \right) \right] \sigma_\infty^2 +
$$

$$
+ \underbrace{\left(\frac{1}{T_1} \frac{\partial T_1}{\partial y^{(i)}} - \frac{1}{T_2} \frac{\partial T_2}{\partial y^{(i)}} \right)}_{c^{(i)} \left(\sigma_0^{(i)} \right)^2 / \sigma_\infty^2} \left(\frac{\partial \sigma_\infty^2}{\partial c^{(r)}} + \sum_{j=2}^{N} \frac{\partial \sigma_\infty^2}{\partial \hat{y}^{(j)}} \frac{\partial \hat{y}^{(j)}}{\partial c^{(r)}} \right) - \left(\sigma_0^{(i)} \right)^2 \delta_{ir} = 0,
$$

$$
\underline{i = 2, 3, \dots, N}, \quad r = 1, 2, 3, \dots, N, \quad \underline{\hat{y}^{(i)} \neq 0}, \quad \text{(A.12)}
$$

or

$$
\sum_{j=2}^{N} \left[\left(-\frac{\partial T_1}{\partial \hat{y}^{(i)}} \frac{\partial T_1}{\partial \hat{y}^{(j)}} \frac{1}{T_1^2} + \frac{\partial^2}{T_1} \partial \hat{y}^{(i)} \partial \hat{y}^{(j)} \frac{1}{T_1} + \frac{\partial T_2}{\partial \hat{y}^{(i)}} \frac{\partial T_2}{\partial \hat{y}^{(j)}} \frac{1}{T_2^2} - \frac{\partial^2 T_2}{\partial \hat{y}^{(i)} \partial \hat{y}^{(j)}} \frac{1}{T_2} \right) \sigma_\infty^2 + \right.
$$

$$
\left. + \frac{\partial \sigma_\infty^2}{\partial \hat{y}^{(j)}} \frac{c^{(i)} \left(\sigma_0^{(i)} \right)^2}{\sigma_\infty^2} \right] \frac{\partial \hat{y}^{(j)}}{\partial c^{(r)}} =
$$

$$
= \left(\frac{\partial T_1}{\partial \hat{y}^{(i)}} \frac{\partial T_1}{\partial c^{(r)}} \frac{1}{T_1^2} - \frac{\partial^2 T_1}{\partial \hat{y}^{(i)} \partial c^{(r)}} \frac{1}{T_1} - \frac{\partial T_2}{\partial \hat{y}^{(i)}} \frac{\partial T_2}{\partial c^{(r)}} \frac{1}{T_2^2} + \frac{\partial^2 T_2}{\partial \hat{y}^{(i)} \partial c^{(r)}} \frac{1}{T_2} \right) \sigma_\infty^2 -
$$

$$
- \frac{\partial \sigma_\infty^2}{\partial c^{(r)}} \frac{c^{(i)} \left(\sigma_0^{(i)} \right)^2}{\sigma_\infty^2} + \left(\sigma_0^{(i)} \right)^2 \delta_{ir},
$$

$$
\underline{i = 2, 3, \dots, N}, \quad r = 1, 2, 3, \dots, N, \quad \underline{\hat{y}^{(i)} \neq 0}. \quad \text{(A.13)}
$$

The above system of equations defines $\frac{\partial \hat{y}^{(j)}}{\partial c^{(r)}}$ for $j = 2, 3, \dots, N$, $r = 1, 2, \dots, N$ and $\hat{y}^{(i)} \neq 0$. Similarly

$$
\frac{\partial A^{(i)}}{\partial \sigma_0^{(r)}} = \left[-\frac{1}{T_1^2} \left(\sum_{j=2}^{N} \frac{\partial T_1}{\partial \hat{y}^{(j)}} \frac{\partial \hat{y}^{(j)}}{\partial \sigma_0^{(r)}} \right) \frac{\partial T_1}{\partial \hat{y}^{(i)}} + \frac{1}{T_1} \left(\sum_{j=2}^{N} \frac{\partial^2 T_1}{\partial \hat{y}^{(j)} \partial \hat{y}^{(i)}} \frac{\partial \hat{y}^{(j)}}{\partial \sigma_0^{(r)}} \right) + \right.
$$

$$
+ \frac{1}{T_2^2} \left(\sum_{j=2}^{N} \frac{\partial T_2}{\partial \hat{y}^{(j)}} \frac{\partial \hat{y}^{(j)}}{\partial \sigma_0^{(r)}} \right) \frac{\partial T_2}{\partial \hat{y}^{(i)}} - \left. \frac{1}{T_2} \left(\sum_{j=2}^{N} \frac{\partial^2 T_2}{\partial \hat{y}^{(j)} \partial \hat{y}^{(i)}} \frac{\partial \hat{y}^{(j)}}{\partial \sigma_0^{(r)}} \right) \right] \sigma_\infty^2 +
$$

$$
+ \underbrace{\left(\frac{1}{T_1} \frac{\partial T_1}{\partial y^{(i)}} - \frac{1}{T_2} \frac{\partial T_2}{\partial y^{(i)}} \right)}_{c^{(i)} \left(\sigma_0^{(i)} \right)^2 / \sigma_\infty^2} \left(\frac{\partial \sigma_\infty^2}{\partial \sigma_0^{(r)}} + \sum_{j=2}^{N} \frac{\partial \sigma_\infty^2}{\partial \hat{y}^{(j)}} \frac{\partial \hat{y}^{(j)}}{\partial \sigma_0^{(r)}} \right) - 2 \, c^{(i)} \, \sigma_0^{(i)} \, \delta_{ir} = 0,
$$

$$
\underline{i = 2, 3, \dots, N}, \quad r = 1, 2, 3, \dots, N, \quad \underline{\hat{y}^{(i)} \neq 0}. \quad \text{(A.14)}
$$

or

$$\sum_{j=2}^{N} \left[\left(-\frac{\partial T_1}{\partial \hat{y}^{(i)}} \frac{\partial T_1}{\partial \hat{y}^{(j)}} \frac{1}{T_1^2} + \frac{\partial^2 T_1}{\partial \hat{y}^{(i)} \partial \hat{y}^{(j)}} \frac{1}{T_1} + \frac{\partial T_2}{\partial \hat{y}^{(i)}} \frac{\partial T_2}{\partial \hat{y}^{(j)}} \frac{1}{T_2^2} - \frac{\partial^2 T_2}{\partial \hat{y}^{(i)} \partial \hat{y}^{(j)}} \frac{1}{T_2} \right) \sigma_\infty^2 + \right.$$

$$\left. + \frac{\partial \sigma_\infty^2}{\partial y^{(j)}} \frac{c^{(i)} \left(\sigma_0^{(i)} \right)^2}{\sigma_\infty^2} \right] \frac{\partial \hat{y}^{(j)}}{\partial \sigma_0^{(r)}} = 2 \, c^{(i)} \, \sigma_0^{(i)} \, \delta_{ir} - \frac{\partial \sigma_\infty^2}{\partial \sigma_0^{(r)}} \frac{c^{(i)} \left(\sigma_0^{(i)} \right)^2}{\sigma_\infty^2},$$

$$\underline{i = 2, 3, \ldots, N, \quad r = 1, 2, 3, \ldots, N, \quad \hat{y}^{(i)} \neq 0.} \tag{A.15}$$

The above system of equations defines $\frac{\partial \hat{y}^{(j)}}{\partial \sigma_0^{(r)}}$ for $j = 2, 3, \ldots, N$,$r = 1, 2, \ldots, N$ and $\hat{y}^{(i)} ne 0$. If one of the optimal values $\hat{y}^{(i)}$ vanishes, the objective function has an unconstrained minimum for negative $y^{(i)}$. In such a case, in view of the continuity of the functions involved, variation of $c^{(r)}$ and $\sigma_0^{(r)}$ changes the value of the unconstrained minimum, which still occurs at some different but still negative $y^{(i)}$. Therefore the $\hat{y}^{(i)}$ for the constrained minimization still vanishes, i.e., if $\hat{y}^{(i)} = 0$, then $\frac{\partial \hat{y}^{(i)}}{\partial c^{(r)}} = 0$ and $\frac{\partial \hat{y}^{(j)}}{\partial \sigma_0^{(r)}} = 0$.

Appendix B

We have that

$$\mathbf{D}^{(i)} = \alpha^{(i)} \mathbf{D}, \qquad \alpha^{(i)} \left(c^{(s)}, y^{(s)} \right) = \frac{F^{(i)} \left(y^{(i)} \right)}{\Pi \left(c^{(s)}, y^{(s)} \right)}, \tag{B.1}$$

$$F^{(i)} \left(y^{(i)} \right) = \frac{y^{(i)}}{3 \, y^{(i)} + 2 \, y_0}, \qquad \Pi \left(c^{(s)}, y^{(s)} \right) = \sum_{s=1}^{N} c^{(s)} \, F \left(y^{(s)} \right). \tag{B.2}$$

Also

$$\dot{\bar{\varepsilon}}^{(i)} = \alpha^{(i)} \left(c^{(r)}, y^{(r)} \right) \dot{\bar{\varepsilon}}, \tag{B.3}$$

where

$$\dot{\bar{\varepsilon}}^{(i)} = \sqrt{\frac{2}{3} \mathbf{D}^{(i)} : \mathbf{D}^{(i)}} \quad \text{(no sum on } i) \qquad \text{and} \qquad \dot{\bar{\varepsilon}} = \sqrt{\frac{2}{3} \mathbf{D} : \mathbf{D}} \, .$$

Variation of $a^{(i)} \left(c^{(r)}, \sigma_0^{(r)} \right)$

$$\alpha^{(i)} \left(c^{(s)}, y^{(s)} \right) = \frac{y^{(i)}}{3 \, y^{(i)} + 2 \, y_0} \left(\sum_{s=1}^{N} \frac{c^{(s)} \, y^{(s)}}{3 \, y^{(s)} + 2 \, y_0} \right)^{-1} = \frac{F^{(i)} \left(y^{(i)}, y_0 \right)}{\Pi \left(c^{(r)}, y^{(r)}, y_0 \right)}, \qquad y_0 = y_0 \left(c^{(r)}, y^{(r)} \right),$$
$$\tag{B.4}$$

$$F^{(i)} \left(y^{(s)}, y_0 \right) = \frac{y^{(i)}}{3 \, y^{(i)} + 2 \, y_0}, \qquad \Pi \left(c^{(s)}, y^{(s)}, y_0 \right) = \sum_{s=1}^{N} \frac{c^{(s)} \, y^{(s)}}{3 \, y^{(s)} + 2 \, y_0} = \sum_{s=1}^{N} c^{(s)} \, F^{(s)} \left(y^{(s)}, y_0 \right).$$
$$\tag{B.5}$$

Evaluation of $\frac{\partial \alpha^{(i)}}{\partial \sigma_0^{(j)}}$

We have that

$$\frac{\partial \alpha^{(i)}}{\partial \sigma_0^{(j)}} = \sum_{k=1}^{N} \frac{\partial \alpha^{(i)}}{\partial y^{(k)}} \frac{\partial y^{(k)}}{\partial \sigma_0^{(j)}} \qquad \Rightarrow \qquad \left[\frac{\partial \alpha^{(i)}}{\partial \sigma_0^{(j)}} \right]_{N \times N} = \left[\frac{\partial \alpha^{(i)}}{\partial y^{(k)}} \right]_{N \times N} \left[\frac{\partial y^{(k)}}{\partial \sigma_0^{(j)}} \right]_{N \times N}. \tag{B.6}$$

Therefore, we need $\frac{\partial \alpha^{(i)}}{\partial y^{(j)}}$, which is determined as follows.

$$\frac{\partial \alpha^{(i)}}{\partial y^{(j)}} = \left(\frac{\partial F^{(i)}}{\partial y^{(j)}} + \frac{\partial F^{(i)}}{\partial y_0} \frac{\partial y_0}{\partial y^{(j)}} \right) \frac{1}{\Pi} - \frac{F^{(i)}}{\Pi^2} \left(\frac{\partial \Pi}{\partial y^{(j)}} + \frac{\partial \Pi}{\partial y_0} \frac{\partial y_0}{\partial y^{(j)}} \right) \qquad \Rightarrow$$

$$\frac{\partial \alpha^{(i)}}{\partial y^{(j)}} = \frac{1}{\Pi} \left[\frac{\partial F^{(i)}}{\partial y^{(j)}} + \frac{\partial F^{(i)}}{\partial y_0} \frac{\partial y_0}{\partial y^{(j)}} - \alpha^{(i)} \left(\frac{\partial \Pi}{\partial y^{(j)}} + \frac{\partial \Pi}{\partial y_0} \frac{\partial y_0}{\partial y^{(j)}} \right) \right], \qquad i, j = 1, 2, \dots, N. \quad (B.7)$$

We need $\frac{\partial F^{(i)}}{\partial y^{(j)}}$, $\frac{\partial F^{(i)}}{\partial y_0}$, $\frac{\partial \Pi}{\partial y^{(j)}}$, $\frac{\partial \Pi}{\partial y_0}$.

Evaluation of $\frac{\partial \alpha^{(i)}}{\partial c^{(j)}}$

$$\frac{\partial \alpha^{(i)}}{\partial c^{(j)}} = \frac{1}{\Pi} \frac{\partial F^{(i)}}{\partial y_0} \frac{\partial y_0}{\partial c^{(j)}} - frac F^{(i)} \Pi^2 \left(\frac{\partial \Pi}{\partial c^{(j)}} + \frac{\partial \Pi}{\partial y_0} \frac{\partial y_0}{\partial c^{(j)}} \right) \qquad \Rightarrow$$

$$\frac{\partial \alpha^{(i)}}{\partial c^{(j)}} = \frac{1}{\Pi} \left[\frac{\partial F^{(i)}}{\partial y_0} \frac{\partial y_0}{\partial c^{(j)}} - \alpha^{(i)} \left(\frac{\partial \Pi}{\partial c^{(j)}} + \frac{\partial \Pi}{\partial y_0} \frac{\partial y_0}{\partial c^{(j)}} \right) \right], \qquad i, j = 1, 2, \dots, N. \quad (B.8)$$

We need $\frac{\partial F^{(i)}}{\partial y_0}$, $\frac{\partial \Pi}{\partial y_0}$, $\frac{\partial \Pi}{\partial c^{(i)}}$.

We have that

$$\frac{\partial F^{(i)}}{\partial y^{(j)}} = \frac{\delta_{ij}}{3\,y^{(i)} + 2\,y_0} - \frac{y^{(i)}}{\left(3\,y^{(i)} + 2\,y_0\right)^2} 3\,\delta_{ij} = \frac{\delta_{ij}}{3\,y^{(i)} + 2\,y_0} \left(1 - \frac{3\,y^{(i)}}{3\,y^{(i)} + 2\,y_0} \right) \qquad \Rightarrow$$

$$\frac{\partial F^{(i)}}{\partial y^{(j)}} = \frac{2\,y_0\,\delta_{ij}}{\left(3\,y^{(i)} + 2\,y_0\right)^2}, \qquad \frac{\partial F^{(i)}}{\partial y_0} = -\frac{2\,y^{(i)}}{\left(3\,y^{(i)} + 2\,y_0\right)^2}. \qquad (B.9)$$

Also

$$\frac{\partial \Pi}{\partial y^{(i)}} = c^{(i)} \frac{\partial F^{(i)}}{\partial y^{(i)}}, \qquad \frac{\partial \Pi}{\partial y_0} = \sum_{i=1}^{N} c^{(i)} \frac{\partial F^{(i)}}{\partial y_0}, \qquad \frac{\partial \Pi}{\partial c^{(i)}} = F^{(i)}.$$

The value of $\frac{\partial y_0}{\partial y^{(j)}}$ depends on the model used.

i) $y_0 = y^{(1)} \qquad \Rightarrow \qquad \frac{\partial y_0}{\partial y^{(i)}} = \delta_{1i} \qquad$ and $\qquad \frac{\partial y_0}{\partial c^{(i)}} = 0,$

ii) $y_0 = \sum_{r=1}^{N} c^{(r)} y^{(r)} \qquad \Rightarrow \qquad \frac{\partial y_0}{\partial y^{(i)}} = c^{(i)} \qquad$ and $\qquad \frac{\partial y_0}{\partial c^{(i)}} = y^{(i)}.$